Learning Interpolation via Regional Map for Pan-Sharpening

Cheng Shi, Fang Liu, *Senior Member, IEEE*, Lingling Li, Licheng Jiao, *Senior Member, IEEE*, Yiping Duan, and Shuang Wang, *Member, IEEE*

***Abstract*—Although the bandwidth of the high-resolution panchromatic (HR PAN) image is wide, it is narrow in each band of the low-resolution multispectral (LR MS) image. Hence, the spatial resolution of the HR PAN image is much higher than that of the LR MS image. However, HR PAN image only has a single band. The purpose of the Pan-sharpening algorithm is to make the Pan-sharpened image with both high spatial resolution and good spectral information. In this paper, a novel learning interpolation method for Pan-sharpening is proposed by expanding the sketch information in the HR PAN image. The sketch information contains the edges and lines features of the image, and each segment of the sketch information has its own direction. According to the primal sketch graph of the HR PAN image, a regional map is obtained by a designed geometrical template. Since the size of the HR PAN image is different from that of the LR MS image, the LR MS image is interpolated into an interpolated multispectral (IMS) image by the nearest interpolation method. In addition, the IMS image can be mapped into the structure and the nonstructure regions by this regional map. The nonstructure regions are divided into the smooth and the texture regions by a variance value. For the structure and texture regions, the interpolated pixels in the IMS image are relearned and readjusted by the proposed structure and texture learning interpolation method, respectively. Experimental results show that the proposed Pan-sharpening method can provide superior performance in both visual effect and quality metrics, particularly for the images with a large spectral difference.**

***Index Terms*—Learning interpolation, pan-sharpening, primal sketch, regional map.**

Manuscript received November 7, 2013; revised March 3, 2014 and September 13, 2014; accepted November 17, 2014. The work was supported in part by the National Basic Research Program (973 Program) of China under Grant 2013CB329402; by the National Natural Science Foundation of China under Grant 61173090, Grant 61173092, Grant 61271302, and Grant 61272282; by the National Research Foundation for the Doctoral Program of Higher Education of China under Grant 20110203110006; by the Fund for Foreign Scholars in University Research and Teaching Programs (the 111 Project) under Grant B07048); by the Program for Cheung Kong Scholars and Innovative Research Team in University under Grant IRT1170; by the Fundamental Research Funds for the Central Universities under Grant JB140317; and by the EU FP7 IRSES Grant under Grant 247619 on "Nature Inspired Computation and its Applications (NICaiA)."

C. Shi, F. Liu, and Y. Duan are with the School of Computer Science and Technology, Xidian University, Xi'an 710071, China, the Key Laboratory of Intelligent Perception and Image Understanding of Ministry of Education, Xi'an 710071, China, and also with the International Research Center for Intelligent Perception and Computation, Xidian University, Xi'an 710071, China (e-mail: f63liu@163.com).

L. Li, L. Jiao, and S. Wang are with the Key Laboratory of Intelligent Perception and Image Understanding of Ministry of Education, Xi'an 710071, China and also with the International Research Center for Intelligent Perception and Computation, Xidian University, Xi'an 710071, China.

Color versions of one or more of the figures in this paper are available online at http://ieeexplore.ieee.org.

Digital Object Identifier 10.1109/TGRS.2014.2375931

I. Introduction

Image fusion refers to the process of combining images from different sensors. If the images to be fused include the low-resolution multispectral(LR MS) image and the high-resolution panchromatic (HR PAN) image, the fusion process is called "Pan-Sharpening" [1], [2].

In the past several years, many Pan-Sharpening methods are present. The classical Pan-Sharpening methods are IHS (Intensity, Hue, and Saturation) [3], [4], PCA (Principal Component Analysis) [5], [6], Gram–Schmidt [7], and Brovery *et al.* [5] transform These methods can improve the spatial effectively information but spectral distortion often appears. To overcome this problem, some popular Pan-sharpening methods are proposed, such as adaptive IHS [8], P+XS [9], wavelet-based method [10], and multiscale geometric analysis (MGA)-based method [11]–[14]. Some MGA tools are widely used in the Pan-Sharpening process, such as Curvelet [11], Bandlet [12], and Contourlet *et al*. [13], [14]. These tools can maintain spectral information better than the classical methods; however, it is impossible for the MGA tools to represent the directions adaptively, which make the balance in spatial resolution difficult.

Recently, the sparse-based method has been gradually studied [15], [16]. Compared with the classical and the optimized Pan-Sharpening algorithm, the proposed Pan-Sharpening results depend on the corrections between the HR PAN image and the injected image. Compared with these methods, the difference of the sparse-based method is that the HR PAN image is not injected into the LR MS image directly (both in the spatial and the frequency domain). The sparse-based method establishes a relationship between the low- and high-resolution images by training a dictionary on a training set, and then according to this relationship, the information of the low-resolution image is used to get its high-resolution version. The sparse-based method gives us a new way for Pan-Sharpening process-improve, but not inject. In this kind of method, the dictionary training is very important. In the method proposed by Li and Yang [15], the dictionary training set was constructed by training the high-resolution MS (HR MS) image and its downsampled image (the low-resolution MS images). However, for a true sensor, the HR MS image (the same resolution with HR PAN image) is impossible to obtain. Zhu and Bamler [16] improved Li's method, the HR PAN and the downsampled LR PAN images are used to train the dictionary. A better Pan-Sharpening result can be obtained for the images with a continuous boundary, but for discontinuous images (images that have rapid changes in details), the detail loss always appears. Thus, the sparse-based method is more suitable for the image with many continuous lines.

"Super-resolution"-based method is based on the LR MS image to get the high-resolution MS image; hence, it can better maintain the spectral information in the Pan-Sharpened image. Meanwhile, the Pan-sharpened result depends on whether the dictionary can better represent the image information or not. In order to overcome the dependence of Pan-Sharpened results on dictionary training and the disadvantage in representing the detail information, the learning interpolation-based Pan-sharpening method is proposed.

Interpolation methods mainly consist of two kinds: the linear-based method and the edge direction-based method. Typical linear interpolation methods include nearest neighbor interpolation, linear interpolation, cubic interpolation, and B-spline interpolation, etc. [17]–[19]. These interpolation methods are simple, but the diffusion phenomenon always appears. Hence, some edge direction-based methods are proposed [20]–[24]. Jensen and Anastassiou [21] gave an edge-directed interpolation method, and Zhou *et al.* [22] proposed an directional cubic convolution interpolation method. These two methods have more complex models, and meanwhile, the interpolation results are affected by the accuracy of edge detection. Giachetti and Asuni [23] proposed an iterative curvature-based interpolation (ICBI) method for real-time applications, and it is suitable for the curvature continuity, curvature enhancement, and isophote contour, but the parameter selection has a great effect on the results. A new edge-directed interpolation (NEDI) method, proposed by Li [24], uses the statistical property of covariance on the edge of the image, and better maintains edge information in the interpolated image. NEDI method has a simple linear prediction model, and does not require the edge detection process.

These interpolation algorithms can maintain better spectral information in the interpolated image, however they are just suitable for continuous lines. In the Pan-sharpening problem, the existence of many discontinuous lines makes it hard to get an ideal spatial resolution in these interpolation methods. Thus a learning interpolation method for Pan-sharpening is proposed. Combine the computer visual model and the Non-local theory, under the guidance of the HR PAN image, the LR MS image is interpolated into the Pan-sharpened image.

This paper is structured as follows. In Section II, the related work is presented. Section III shows the proposed Pan-sharpening algorithm. Experimental results and parameter analysis is done in Section IV. Finally, we conclude a brief summary in Section V.

II. Related Work

Consider the following interpolation model (assume the size of the high-resolution image is two times that of the low-resolution image):

$$f_{HR}(2i+1, 2j+1) = \sum_{k=0}^{1}\sum_{l=0}^{1} \alpha_{2k+l} f_{HR}\left(2(i+k), 2(j+l)\right) \quad (1)$$

where f_{LR} (with size $W \times H$) is a low-resolution image, and f_{HR} (with size $2W \times 2H$)is the high-resolution image of f_{LR}, such as $f_{HR}(2i, 2j) = f_{LR}(i, j)$ $(i = 1, \ldots, W,\ j = 1, \ldots, H)$.

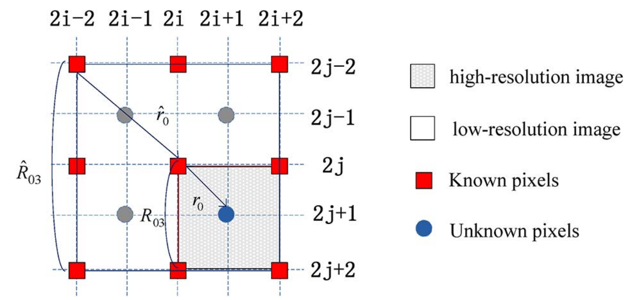

Fig. 1. Geometric regularity for low- and high-resolution images.

$\vec{\alpha} = \alpha_{2k+l}|_{\substack{k=0,1\\ l=0,1}} = (\alpha_0, \alpha_1, \alpha_2, \alpha_3)^T$ represents the weight vector. Equation (1) is used to estimate the pixel values $f_{HR}(2i+1, 2j+1)$ by weighting its four neighborhood pixels that come from the low-resolution image. The NEDI method consists of two steps, the first step is to estimate the pixels $f_{HR}(2i+1, 2j+1)$, and the second one is to estimate the pixels $f_{HR}(2i+1, 2j)$ and $f_{HR}(2i, 2j+1)$. In the first step, the pixels at position $(2i, 2j)$ are called "known pixels" in this paper, and the other pixels are called "unknown pixels." Moreover, in the second step, the pixels at position $(2i, 2j)$ and $(2i+1, 2j+1)$ are called "known pixels," and the other pixels are called "unknown pixels." In the following, we will describe the calculation of $f_{HR}(2i+1, 2j+1)$.

The problem now is how to compute the weight $\vec{\alpha}$, that is, to say how to estimate the pixel $f_{HR}(2i+1, 2j+1)$. The weight $\vec{\alpha}$ plays an important role in the interpolation process. NEDI method is proposed by Li and Orchard[24]. It uses the statistical property of the edge information and the geometric duality of the low- and high-resolution images. Only the low-resolution image is used to estimate the high-resolution image. The interpolation process is adaptive, and it has great advantages in interpolating images with continual edges. Now, the weight computation in the NEDI method is described as follows.

According to the classical Wiener filter theory, the optimal MMSE linear interpolation coefficients can be presented as

$$\vec{\alpha} = R^{-1}\vec{r} \quad (2)$$

where $\vec{\alpha}$ is a weight vector, and R is a covariance matrix of the four-order neighborhood of $f_{HR}(2i+1, 2j+1)$. $[R_{kl}](0 \leq k, l \leq 3)$ contains 16 values, and $\vec{r}$ is the cross-covariance matrix, which contains four elements. For example, $R_{03} = E[f_{HR}(2i, 2j), f_{HR}(2i, 2j+2)]$, and $r_0 = E[f_{HR}(2i, 2j), f_{HR}(2i+1, 2j+1)]$.

According to (2), the weight $\vec{\alpha}$ can be obtained. However, the problem is that $f_{HR}(2i+1, 2j+1)$ is an unknown pixel. In this case, how can we know the high-resolution covariance when we only have a low-resolution image? In [24], Li and Orchard considered that the edges of the high- and the low-resolution images have a property called "geometric regularity." We can replace the value of R and r in the high-resolution image by the $\hat{R}$ and $\hat{r}$ in the low-resolution image. The computation process of $\hat{R}$ and $\hat{r}$ is shown in Fig. 1. According to

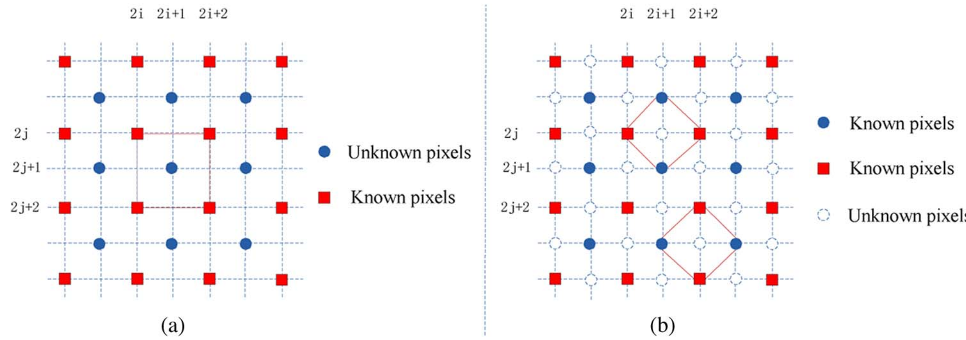

Fig. 2. Interpolation process by NEDI [(a) and (b) are the high-resolution images]. (a) First step for NEDI. (b) Second step for NEDI.

this property, the high-resolution covariance $\hat{R}$ and the cross-covariance matrix $\hat{r}$ can be obtained by the classical covariance method. Then, $\hat{R}$ and $\hat{r}$ can be calculated by

$$\hat{R} = \frac{1}{M^2} C^T C \quad \hat{\vec{r}} = \frac{1}{M^2} C^T \vec{y} \tag{3}$$

where $N \times N$ is the size of a local window used to train the weight. $\vec{y} = [y_1, y_2, \ldots, y_{\mathrm{M}^2}]^T$ is the known pixels in the window, C is a matrix with size $\mathrm{M}^2 \times 4$ (M is the number of the known pixels in the local window), and the kth row of C is the four neighborhood-known pixels of y_k. By training the weight for each known pixel in the local window, and according to (2) and (3), the weight $\vec{\alpha}$ can be calculated by

$$\vec{\alpha} = (C^T C)^{-1} (C^T \vec{y}). \tag{4}$$

Equation (1) shows how to estimate the pixel $f_{HR}(2i+1, 2j+1)$. The second step is to estimate the other unknown pixels ($f_{HR}(2i+1, 2j)$ and $f_{HR}(2i, 2j+1)$). There is a process similar to the aforementioned step. Rotate the training window by 45° to select the neighborhood pixels, and calculate the weight $\vec{\alpha}$ according to (4) (more details can be found in [24]). Fig. 2 shows the interpolation process of NEDI.

III. Learning Interpolation Based on Regional Map

NEDI can better maintain spectral information in the interpolated image, making it very suitable for the Pan-sharpening problem. However, all the interpolation algorithms are more suitable for the image with continuous boundary, but for the discontinuous edges, a minor change in the interpolated image may be ignored. Hence, it cannot satisfy the spatial resolution requirement in the Pan-sharpening problem. In the Pan-sharpening problem, minor details are also important to the following processing. To construct the interpolated image more precisely, the learning interpolation model is designed and shown in (5)

$$f_{HR}(2i+1, 2j+1) = \sum_{k=0}^{1} \sum_{l=0}^{1} \alpha_{2k+l} f_{HR}(2(i+k), 2(j+l)) + \delta(2i+1, 2j+1). \tag{5}$$

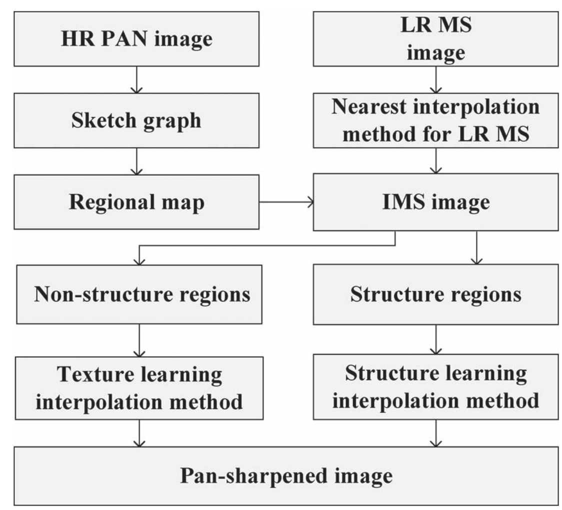

Fig. 3. Block diagram of learning interpolation via regional map for Pan-sharpening (Assume the size of the HR PAN image is two times larger than the LR MS image).

Equation (5) is an improvement of (1). f_{HR} is the Pan-sharpened HR MS image, and δ is an adjustment parameter, which reflects the difference between the Pan-sharpened HR MS image and the predicted interpolated image (the image is interpolated only by weight parameter α_{2k+l}). Similar to NEDI, the learning interpolation model consists of two steps, the first step is to estimate the pixel $f_{HR}(2i+1, 2j+1)$, and the second step is to estimate $f_{HR}(2i+1, 2j)$ and $f_{HR}(2i, 2j+1)$. For each step, the learning interpolation consists of three parts: regional division, the weight parameter estimation, adjustment of the learning interpolation pixels under the guidance of HR PAN image. The learning interpolation algorithm can only enlarge the low-resolution image twice. Hence, in the sections of regional division, weight learning, and adjustment parameter learning, we assume that the size of the HR PAN image is two times that of the LR MS image. The block diagram of the learning interpolation is shown in Fig. 3. In the following sections, we describe each part in detail.

A. Regional Division for IMS Image According to the Regional Map of HR PAN Image

Marr proposed the concept of "primal sketch" [25]. He thought that the image can be divided into two components, "sketchable" and " nonsketchable" parts. The "sketchable" part

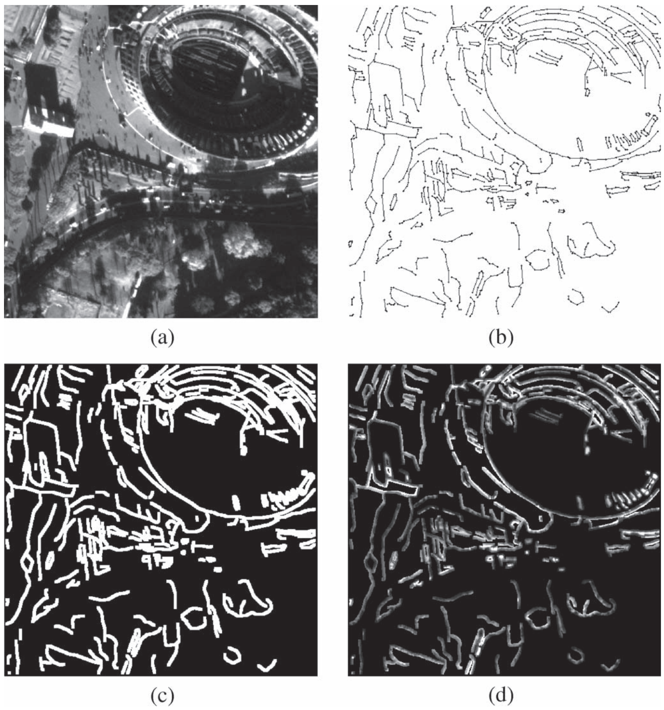

Fig. 4. Sketch graph and structure division. (a) Original HR PAN image. (b) Sketch graph. (c) Regional map (concept-map, which reflects the regions where the lines and edges lie in. The white region is the structure region, and the black region is the nonstructure region, and the size of the template is 7×7). (d) Extracted structure regions of (a) (The structure regions are mapped into the original image, and nonstructure regions are marked as black color).

just contains the structure of the image, and the " nonsketchable" part contains the texture and smooth regions. People always focus on the primal sketch of the image, for it contains the key information about the image sense. Marr has done a lot of objective description for primal sketch, but no explicit mathematical model was given. In 2003, Zhu gave a theoretical model of the primal sketch in the International Computer Vision Conference [26], [27], which is different from the traditional edge detection algorithm; the sketch graph is constructed by the segments with directions. The main steps are shown as follows.

1. Take the convolution operations on the input image by the Gauss-order differential filter and Gaussian second-order differential filter, respectively.
2. Fuse the filtered images to obtain the energy diagram, which reflects the brightness variations of the image.
3. Obtain an initial sketch graph by using the nonmaxima suppression algorithm on the energy diagram.
4. The final Primal Sketch graph can be obtained by the greedy pursuit algorithm and a group of graph operators.

Fig. 4(b) shows the sketch graph of the HR PAN image. The segment in the sketch graph only has a single pixel; however, the edges of the image have a certain width. Therefore, along the direction of each segment, a template is designed to represent the geometric structure block of the image. The pixels in the same line have the same direction, and each pixel in one geometric structure block has the same direction.

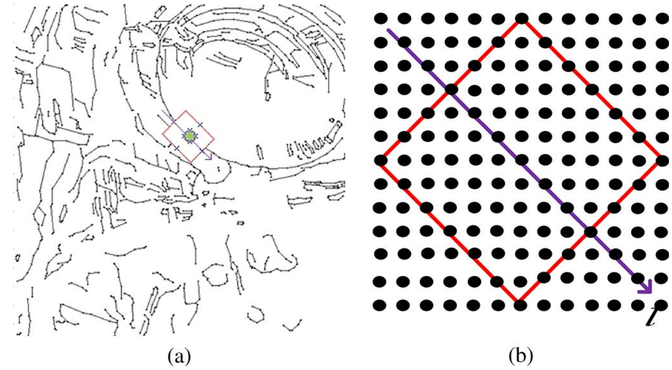

Fig. 5. Designed template for constructing the regional map (a) Designed template in Sketch graph (The red window is the selected window with center at the green pixel). (b) Designed geometric template for the segment l (the block circle is represent the each pixel in the original image).

According to the designed template, the image can be divided into the structure and the nonstructure regions [see Fig. 4(d)]. The binary map of the structure and the nonstructure regions is called "regional map" in this paper. Fig. 5 shows the designed template and Fig. 4(c) gives the regional map.

The variance value reflects the statistical properties of the image. For the nonstructure regions, when the variance value is less than a certain threshold T, the region has small changes in gradient value, and then, we call it "smooth region"; otherwise, the region is called "texture region." Now, the image can be divided into the structure, texture, and smooth regions.

For the Pan-sharpening problem, the regional map and the variance calculation are obtained from the HR PAN image. Since the HR PAN image has a different size with the LR MS image, the LR MS image is first interpolated into an interpolated multispectral (IMS) image by the nearest interpolation method (copy the value of each pixel of the LR MS image to its neighborhood pixels to get the IMS image). The IMS image has the same size with HR PAN image. In addition, according to the regional map and the variance value obtained by HR PAN image, the IMS image is mapped into structure, texture, and smooth regions. In the following sections, the pixels in the position of $(2i+1, 2j+1)$, $(2i+1, 2j)$, and $(2i, 2j+1)$ in the IMS image will be reestimated to get a more accurate interpolated pixel.

B. Estimate the Weight Parameter

In the traditional NEDI algorithm, only the local window is used to compose the training set in the training process (the process aims to form the matrix C). However, the pixels in the local window may not have the similar structures. Hence, the error of the training set will lead to the calculation error of $\vec{\alpha}$. In order to estimate the weight parameter $\vec{\alpha}$ more precisely, the global information should be considered. The nonlocal idea has been successfully applied to image denoising [28]–[31]. It can maintain the edge and texture information better. This idea can also be applied to learning the interpolation weight. In our interpolation problem, these similar blocks should have a similar weight. Hence, all the blocks, similar to the interpolated

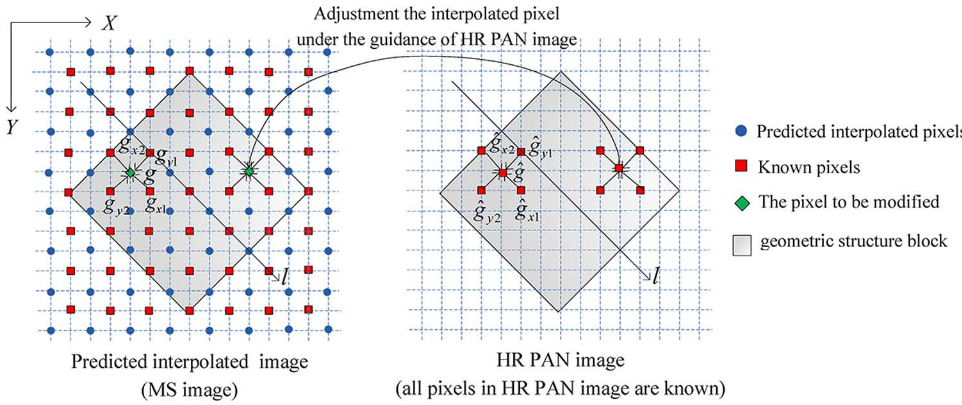

Fig. 6. Adjustment learning for the structure regions (l is the segment in the primal sketch graph).

pixel, are searched to form the matrix C (we call it "weight training set"), and then the weight is learned according to (4). Now, the problem to be solved is the high computational complexity of the nonlocal search. It is hard to achieve a real global search, and thus a fast global search algorithm based on the direction of the geometric structure block is proposed.

In section A, the IMS image can be divided into the structure, texture and smooth regions. Each segment has its direction in the structure region. Similar blocks should have a similar direction. If the interpolated pixel (the pixels in the position of $(2i+1, 2j+1)$ in the first step, or $(2i+1, 2j)$ and $(2i, 2j+1)$ in the second step) is in the structure regions, its directions can be considered as the direction of its four neighborhood-known pixels. Thus its similar blocks can be obtained by calculating the similarity with the same direction blocks. In addition, the weight can be learned according to these similar blocks. If the interpolated pixel is in the nonstructure regions, two cases should be considered. For the smooth region, the weight is $\vec{\alpha} = [0.25, 0.25, 0.25, 0.25]$, and for the texture region, the weight is estimated by the NEDI algorithm.

After learning the weight parameter $\vec{\alpha}$, the pixel to be reinterpolated in the IMS image can be estimated by linear weighting its four neighborhood pixels (similar process to NEDI). In the following sections, the linear weighted pixel is called "predicted interpolated pixel."

C. Adjustment of the Predicted Learning Interpolation Pixels Under the Guidance of HR PAN Image

The predicted interpolated image better maintains spectral information. However, the details may not be accurate, particularly for the minor details. To further improve the detail information in the Pan-sharpened image, it is necessary to make an adjustment parameter δ to the predicted interpolated pixel. The idea of the adjustment parameter learning comes from the Poisson equation-based image recovery. Lin *et al.* [32] proposed a cloud cloning algorithm in their paper. The basic idea is to clone information from cloud-free patches to their corresponding cloud-contaminated patches in several images (These images are obtained from different time, but for the same place). The cloud-contaminated patches can be recovered according to the gradient field provided by the cloud-free patches. Meanwhile, the boundary in the cloud-contaminated patches is unchanged. The boundary condition can maintain the spectral information of the cloud-contaminated image. The adjustment parameter δ cannot be obtained if we only have the LR MS image. However, in the Pan-sharpening problem, we have the HR PAN image that has a similar structure with the Pan-sharpened image. Thus, the gradient information of the HR PAN image is considered when estimating δ. The solution of the Poisson equation has high computational complexity, and in the proposed Pan-sharpening algorithm, only one interpolated pixel needs to be adjusted for each time. Therefore, the process can be simplified. The proposed method to estimate the adjustment parameter δ is to add δ to the predicted interpolated pixel, and make the predicted interpolated image of a similar gradient value with the HR PAN image. Hence, the adjust model is

$$\min_{\delta} \left\{ (f_x(\delta) - \lambda_1 \hat{f}_x)^2 + (f_y(\delta) - \lambda_2 \hat{f}_y)^2 \right\} \tag{6}$$

where f_x and f_y represent the gradient function calculated in the predicted interpolated image along the different directions. The variable of the function is the parameter δ. In addition, $\hat{f}_x$ and $\hat{f}_y$ mean the gradient value in the HR PAN image. λ_1 and λ_2 are the intensity parameters that determine the intensity of the adjustment. Too large of the values λ_1 and λ_2 will result in an artificial phenomenon in the Pan-sharpened image; however, too small of their values will lead to the image blur. Thus, the parameters λ_1 and λ_2 are set to adjust the gradient value of the HR PAN image. The parameters λ_1 and λ_2 are calculated in

$$\begin{aligned} \lambda_1 &= (g_{x1} - g_{x2})/(\hat{g}_{x1} - \hat{g}_{x2}) \\ \lambda_2 &= (g_{y1} - g_{y2})/(\hat{g}_{y1} - \hat{g}_{y2}) \end{aligned} \tag{7}$$

where g_{x1} and g_{x2} are the neighborhood-known pixels in the predicted interpolated image, which are searched along the gradient computation direction of f_x. $\hat{g}_{x1}$ and $\hat{g}_{x2}$ are the pixel values in the HR PAN image, which have the same position with g_{x1} and g_{x2}. If $\hat{g}_{x1} = \hat{g}_{x2}$, $\lambda_1 = 1$, and if $\hat{g}_{y1} = \hat{g}_{y2}$, $\lambda_2 = 1$. The positions of these four pixels are shown in Fig. 6.

Now, we describe the direction selection when calculating the gradient function f_x and f_y. By the regional map, the IMS image can be divided into the structure and the nonstructure regions. In the structure region, edge direction can be obtained by the direction of the geometric structure block. Along the edge direction, the changes in gray value are continuous, and perpendicular to the edge direction, the gradient is changed dramatically. The aim of computing parameter δ is to keep the continuous information along the edge direction, and modify the detail information perpendicular to the edge direction. Hence, for the structure region, f_x is calculated along the edge direction, and f_y is calculated perpendicular to the edge direction. The first term in (6) can be considered as the smooth term, and the second means the gradient modify term. The coordinate direction is shown in Fig. 6. In the texture region, f_x is calculated along the 45° in the first interpolation step, and 0° in the second step.

After determining the gradient computation directions, add the parameter δ to the predicted interpolated pixel, and obtain the gradient functions f_x and f_y, respectively. In addition, compute the gradient values $\hat{f}_x$ and $\hat{f}_y$ in the HR PAN image. f_x, f_y, $\hat{f}_x$, and $\hat{f}_y$ are calculated in

$$\begin{aligned} f_x(\delta) &= g_{x1} + g_{x2} - 2(g+\delta) \quad \hat{f}_x = \hat{g}_{x1} + \hat{g}_{x2} - 2\hat{g} \\ f_y(\delta) &= g_{y1} + g_{y2} - 2(g+\delta) \quad \hat{f}_y = \hat{g}_{y1} + \hat{g}_{y2} - 2\hat{g} \end{aligned} \tag{8}$$

where g is the predicted interpolated pixel in the IMS image, and $\hat{g}$ is the pixel in the HR PAN image, which has the same position with g. Equation (6) is a minimization problem, and each term in (6) is a quadratic function; hence, its solution can be easily derived by assuming the first-order derivative of the relative objective function equals to zero.

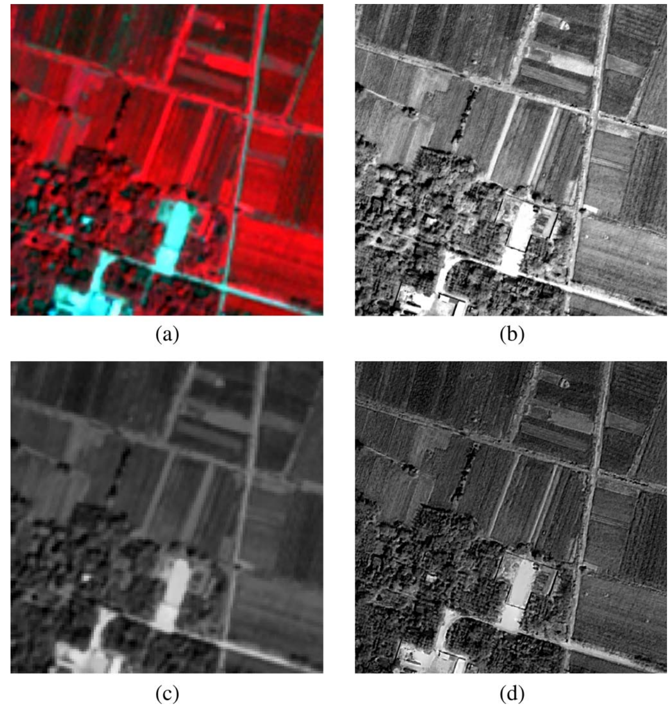

Fig. 7. Learning interpolation for the intensity component of the LR MS image. (a) LR MS image. (b) HR PAN image. (c) Intensity component of the LR MS image. (d) New intensity component after learning interpolation process.

D. Proposed Pan-Sharpening Algorithm-Based on Learning Interpolation and Regional Map

Using the sketch information of the HR PAN image, the regional map and geometric structure block are obtained. It is worth mentioning that the size of the HR PAN image is four times that of the LR MS image for most satellite images; hence, the aforementioned learning interpolation process should be repeated twice. For the first time, the regional map and the HR PAN image are obtained by downsampling the real regional map and original HR PAN image, respectively. For each interpolation process, it consists of two steps, and the first step is to estimate the pixel $f_{HR}(2i+1, 2j+1)$, and the second step is to estimate $f_{HR}(2i, 2j+1)$ and $f_{HR}(2i+1, 2j)$.

In the first step, the interpolated pixel value at position $(2i+1, 2j+1)$ is learned by the learning interpolation method. After the first step, more accurate pixel values at position $(2i+1, 2j+1)$ can be obtained. In the second step, the pixels $f_{HR}(2i, 2j+1)$ and $f_{HR}(2i+1, 2j)$ are estimated based on the result obtained in the first step. From Fig. 2(b), we can see that the second interpolation step is to rotate the training window by 45°. Repeat the learning process twice until all the pixels are interpolated.

The proposed Pan-sharpening algorithm makes full use of the advantage that the spectral information can be kept well before and after the LR MS image is interpolated. In addition, according to the adjustment process, high-resolution Pan-sharpened image can be obtained. Fig. 7 shows an example of modification process. Fig. 7(a) is the LR MS image, and Fig. 7(b) is the HR PAN image. Fig. 7(c) is the intensity component of the LR MS image (obtained by HIS transform). Fig. 7(d) is the modified image by the LIPM model. From Fig. 7(b) and (c), we can see that the HR PAN image has a great difference in spectral information compared with the LR MS image. If the intensity component is substituted by the HR PAN image (or the details of the PAN image) directly, significant distortion will appear in the Pan-Sharpened image. Fig. 7(d) has a better clarity; meanwhile, it has similar spectral information with Fig. 7(c). The block diagram is shown in Fig. 7.

IV. Performance Evaluation

The proposed method for Pan-Sharpening is evaluated in this section. A series of simulation experiments are done using the QuickBird, WorldView-II, and IKONOS images that are from the Internet (http://glcf.umd.edu/data/). Fig. 8 shows the original LR MS and the HR PAN images. The size of the LR MS image is 128 × 128, and the size of the HR PAN image is 512 × 512. For the QuickBird image, the resolution of the LR MS image is 2.44 m, and the resolution of the HR PAN image is 0.61 m. For the WorldView-II image, the size of the LR MS image and the HR PAN images are 2 and 0.5 m, respectively. For the IKONOS image, the size of the LR MS image and the HR PAN images are 4 and 1 m, respectively.

Many well-known quality metrics for spectral information and spatial resolution are used to evaluate the effective of the proposed Pan-sharpening algorithm.

- Quality metrics for spectral information: Relative dimensionless global error in synthesis (ERGAS) [33], correlation coefficient (CC), spectral angle mapper (SAM) [34],

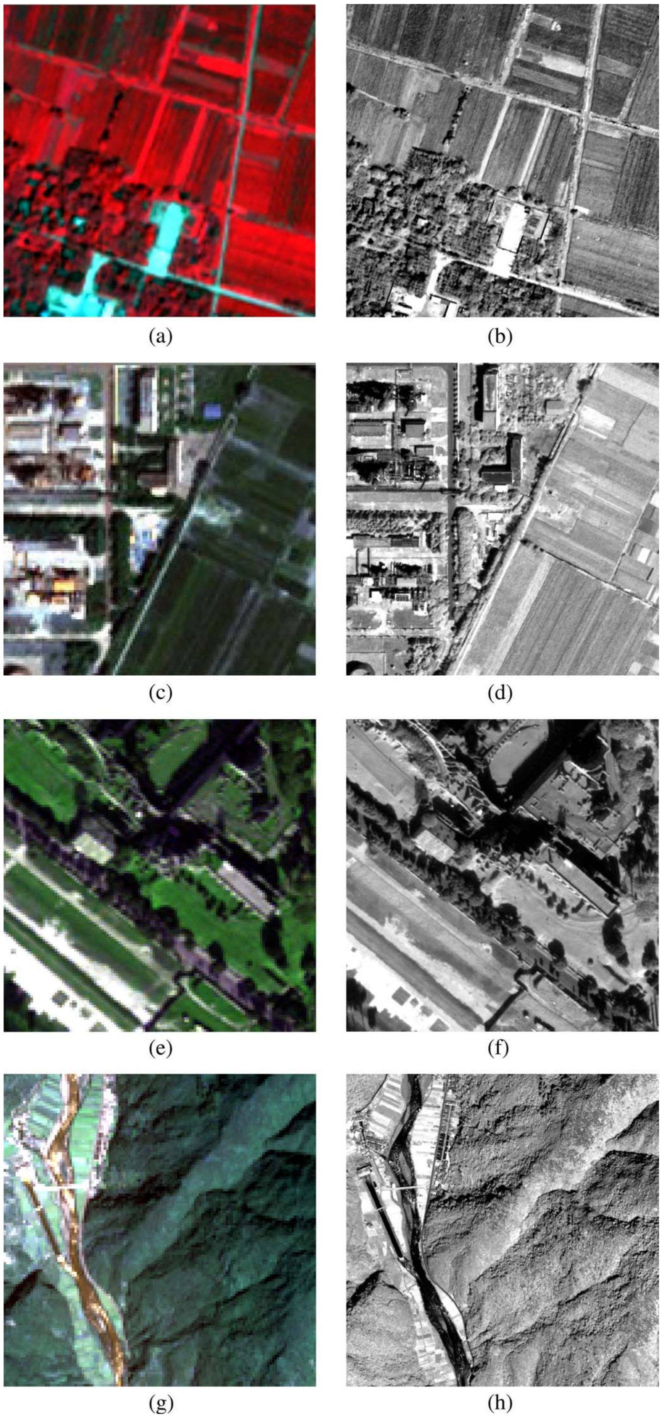

Fig. 8. Original LR MS and HR PAN image. (a) and (b) LR MS and HR PAN QuickBird image of dataset 1. (c) and (d) LR MS and HR PAN QuickBird image of dataset 2. (e) and (f) LR MS and HR PAN WordView-II image of dataset 3. (g) and (h) LR MS and HR PAN IKONOS image of dataset 4.

and spectral information divergence (SID) are used to evaluate the spectral quality.

- Quality metrics for spatial resolution: Peak signal-to-noise ratio (PSNR), and spatial CC (sCC, compare the CC for the high-frequency between the Pan-sharpened image and HR PAN image) [35]) are used to evaluate the spatial resolution of the Pan-sharpened image.

Algorithm 3.1 The proposed Pan-sharpening algorithm

Input: HR PAN and LR MS image (Assume the size of the HR PAN image is four times larger than the LR MS image.)
Output: HR MS image

1. Take the real sketch graph to the original HR PAN image.
2. Downsample the real sketch graph and original HR PAN image, respectively. (The size of the downsampled sketch graph and the HR PAN image is one half of its original). According to the downsampled sketch graph and the downsampled HR PAN image, the regional map is obtained by the designed template.
3. Regional division. Interpolate the LR MS (IMS) image by the nearest interpolation method (the same size with the downsampled HR PAN image). Divide the IMS image into structure, texture and the smooth regions.
4. Learning interpolation. For each band of LR MS image, relearn and readjust the pixels in the structure regions by the structure learning interpolation method, the pixels in the texture regions by the texture learning interpolation method, and the pixels in the smooth regions by the average weighted interpolation method.
5. Interpolation the image obtained from step 4 by the nearest interpolation method, a new IMS image is obtained (the same size with the original HR PAN image). According to the real sketch graph and the real HR PAN image, repeat the learning interpolation process for the new IMS image to get the final Pan-sharpened image.

The method used to evaluate the spectral information of the Pan-sharpened results compares the degraded version of the Pan-sharpened results with the original LR MS image. In addition, the spatial metrics are extracted by using the Pan-sharpened and the original HR PAN images.

A. Selection of Threshold T (Divide the Nonstructure Regions Into Smooth and Texture Regions)

Three groups of experiments are done for the threshold selection. If the variance value for a region is less than threshold T, this region is considered as the smooth region, and the weight is set as $\vec{\alpha} = [0.25, 0.25, 0.25, 0.25]$ directly. In order to determine the threshold value, the HR PAN image and the Pan-sharpened images are filtered using a Laplacian filter, respectively. In addition, the correlation coefficients are computed between each filtered band of the Pan-sharpened image and the filtered HR PAN image. Through the filtering process, the detail information can be presented better in the filtered image. The larger the threshold value, the more blurred the Pan-sharpened images, and the average CC becomes less. Fig. 9(a)–(c) shows the CC statistic graph for the three groups of experiments. The abscissa is the variance value, and the ordinate is the correlation coefficients values. Moreover, Fig. 9(d)–(e) show the variance statistic graph. The abscissa represents the variance value, and the ordinate represents the pixel numbers. As shown

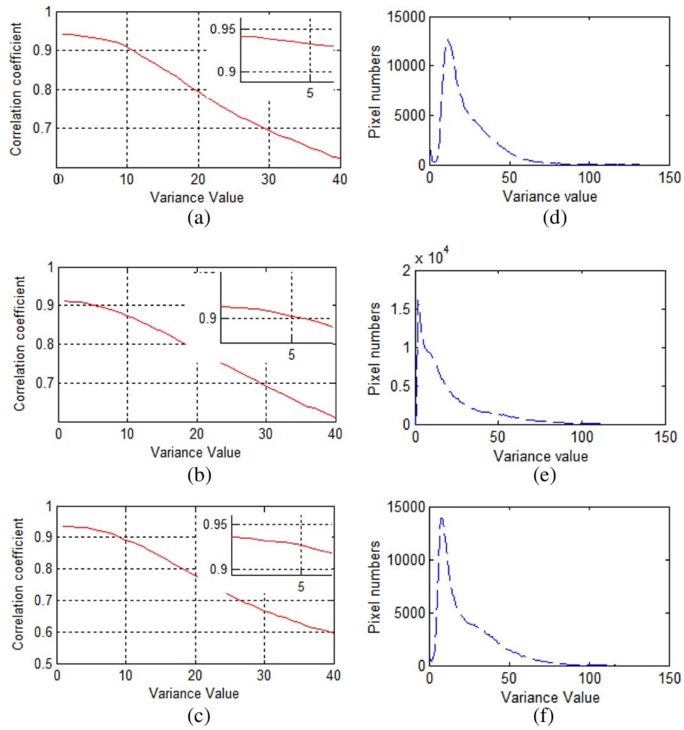

Fig. 9. Statistic map for the three group experiments. (a) CC statistic graph for the first group images. (b) CC statistic graph for the second group images. (c) CC statistic graph for the third group images. (d) Variance statistic map for the first group images. (e) Variance statistic map for the second group images. (f) Variance statistic map for the third group images.

in Fig. 9(d)–(e), most pixels have less variance values. Hence, a larger threshold value can reduce the computation complexity effectively. However, in Fig. 9(a)–(c), the spatial resolution of the Pan-sharpened image decreases with an increased threshold value. When the threshold value is equal to 5, all the CC values in the test images are larger than 0.9. In order to maintain a better spatial resolution, the threshold value is selected as 5 in this paper.

B. Comparative Experiments

To show the effect of the proposed Pan-sharpening algorithm, several different algorithms are compared with the proposed algorithm in their spectral and spatial quality, such as Traditional HIS [4], Adaptive IHS [8], PCA, Sparse FI [16], generalized Laplacian pyramids (GLPs) [36], Wavelet-based Pan-sharpening algorithm [10], UNB-PanSharp [37], and GS-based algorithm [7]. The IHS method is widely used because of its simple computation. In Figs. 10–13, the IHS method can improve the spatial resolution effectively; however, the spectral information is seriously distorted. Particularly in Fig. 11, this problem is even more serious. Similar to IHS method, this problem also appears in the PCA method. Hence, some modification algorithms have been proposed to enhance the spectral information, such as Adaptive IHS. The adaptive IHS method is proposed by Rahmani [8], and from Figs. 10(b) and 12(b), Adaptive IHS produces an image whose spectral information is maintained better than the traditional IHS method, but it is still not ideal. Sparse FI method depends on the trained dictionary, and therefore the results are not stable. In Figs. 10(d)–13(d), the sparse FI method always obtains a better spectral information, however, in Fig. 10(d), the spatial resolution is poor. MRA-based Pan-sharpening algorithm, GLP and Wavelet, can maintain better spectral information in the Pan-sharpened image, particularly for the GLP algorithm, the spatial resolution is maintained as well. Figs. 10–13(g) show the Pan-sharpened image by the UNB-Pansharp algorithm. This algorithm is used in a “Fuze Go” software. UNB-Pansharp has an excellent effect in spatial resolution, however, presents serious loss in the test dates. Similar to the UNB-Pansharp algorithm, the GS-based algorithm is also used in satellite software, such as ENVI. The Pan-sharpened image by the GS algorithm is obtained by the ENVI software. The phenomenon for spectral distortion still exists in the Pan-sharpened image. From the visual aspect, the proposed algorithm has the best effect in balancing the spectral and spatial resolution. It maintains the details clearer than other methods do, and meanwhile, the color is better matched with the LR MS image.

Tables I–IV show the quality metrics of different Pan-Sharpening methods. In Table I, Sparse FI method has a better quality metrics in spectral information. This is because the dictionary is trained only in the HR PAN and downsampled HRPAN image, but the first test image has few line features, and therefore, the trained dictionary cannot represent the image well. Hence, the Pan-sharpened image by Sparse FI method has a poor spatial resolution. Compared with other methods, the proposed Pan-sharpening algorithm reaches the optimum in most values. In these quality metrics, HIS, AIHS, PCA, UNB-Sharpen, and GS algorithm always have higher values in sCC value than the Wavelet and GLP algorithm. However, they fail to get the values in ERGAS, CC, SAM, and SID. Wavelet and GLP algorithm always obtain better values in spectral

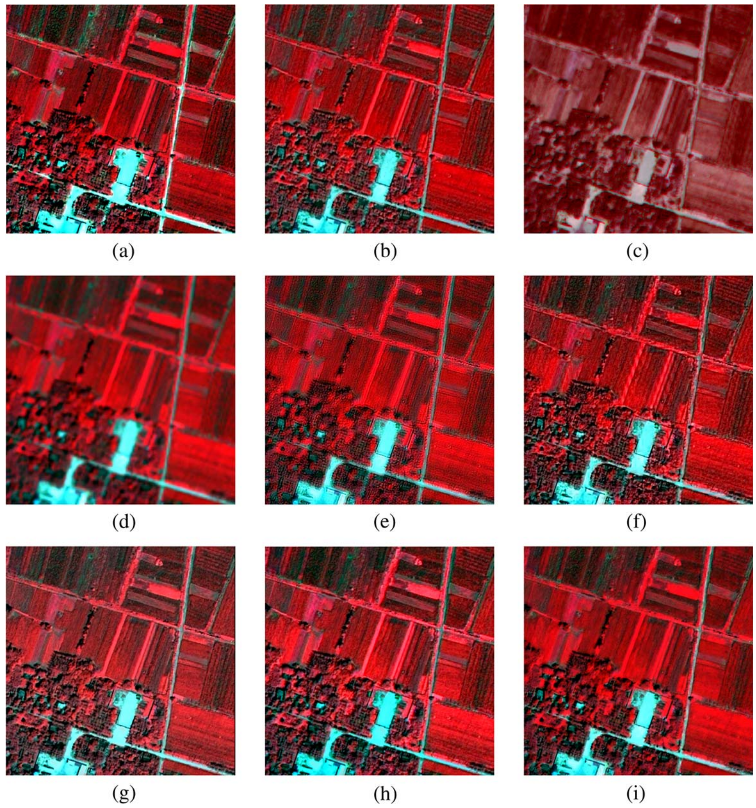

Fig. 10. Pan-sharpening results on dataset 1. (a) Traditional IHS. (b) Adaptive IHS. (c) PCA. (d) Sparse FI. (e) GLP. (f) Wavelet. (g) UNB-PanSharp. (h) GS. (i) Proposed.

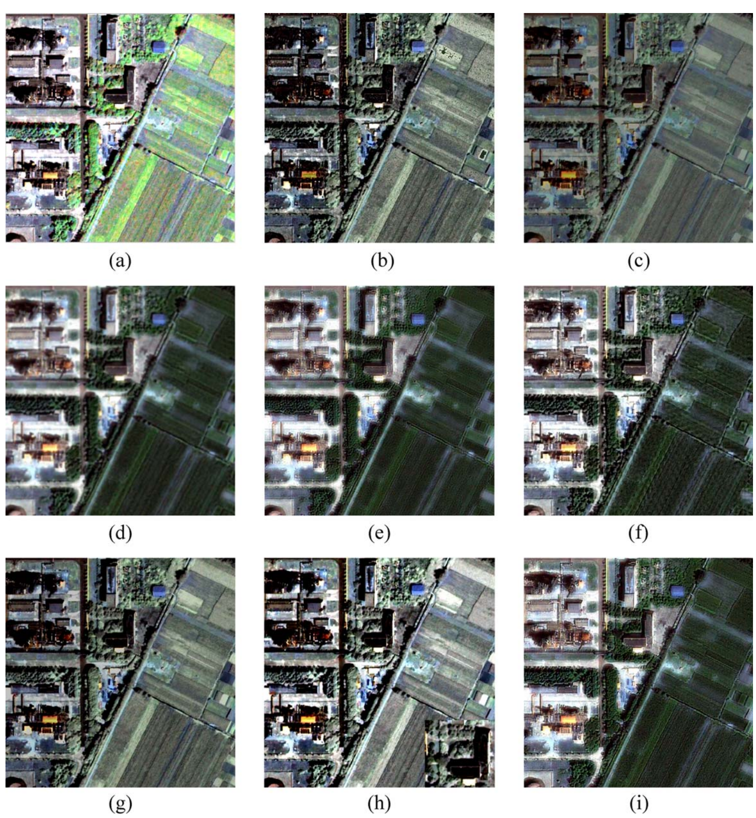

Fig. 11. Pan-sharpening results on dataset 2. (a) Traditional IHS. (b) Adaptive IHS. (c) PCA. (d) Sparse FI. (e) GLP. (f) Wavelet. (g) UNB-PanSharp. (h) GS. (i) Proposed.

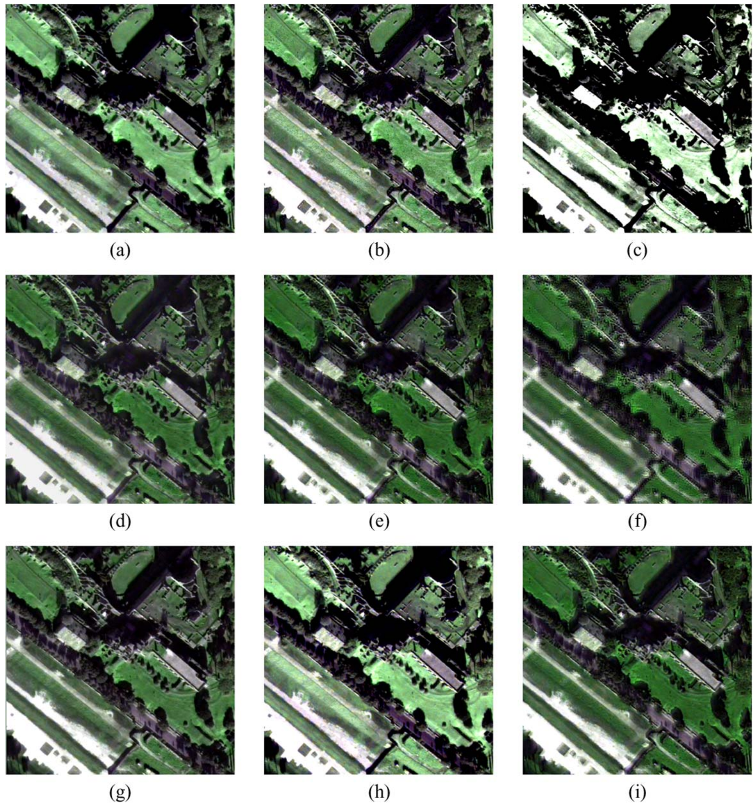

Fig. 12. Pan-sharpening results on dataset 3. (a) Traditional IHS. (b) Adaptive IHS. (c) PCA. (d) Sparse FI. (e) GLP. (f) Wavelet. (g) UNB-PanSharp. (h) GS. (i) proposed.

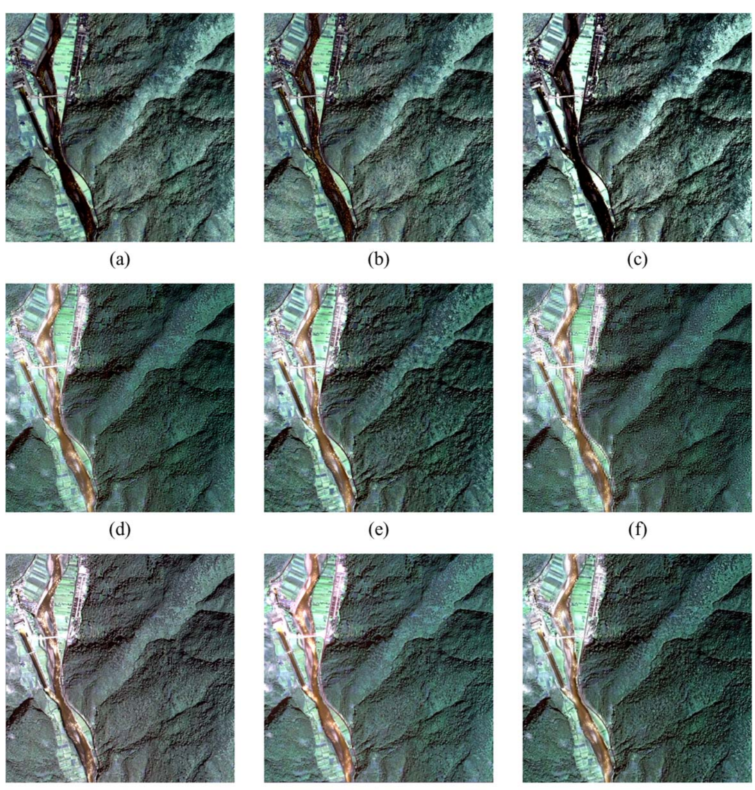

Fig. 13 Pan-sharpening results on dataset 4. (a) Traditional IHS. (b) Adaptive IHS. (c) PCA. (d) Sparse FI. (e) GLP. (f) Wavelet. (g) UNB-PanSharp. (h) GS. (i) Proposed.

TABLE I
QUALITY METRIC IN DATASET I

	ERGAS	CC	SAM	SID	PSNR	sCC
Best Values	0	1	0	0	$+\infty$	1
IHS	4.4593	0.8787	8.8617	0.2534	18.6738	0.8132
AIHS	3.8563	0.9159	2.0813	0.2837	21.9518	0.8877
PCA	7.2266	0.6073	21.8065	2.1444	15.5152	0.7613
Sparse FI	**2.3287**	0.9510	**1.6837**	0.0477	15.2684	0.2186
GLP	2.6871	0.9508	2.9998	0.0728	22.0517	0.9187
Wavelet	4.0556	0.8609	8.9972	0.5860	20.8035	0.8676
UNB-PanSharp	3.7594	0.8929	12.6883	0.2516	18.8695	0.9202
GS	3.8725	0.9024	11.3415	0.2056	20.3503	0.8131
Proposed	2.6173	**0.9514**	1.7228	**0.0425**	**23.9979**	**0.9251**

TABLE II
QUALITY METRIC IN DATASET II

	ERGAS	CC	SAM	SID	PSNR	sCC
Best Values	0	1	0	0	$+\infty$	1
IHS	5.2510	0.4430	7.3449	0.1840	9.1928	0.9217
AIHS	6.5428	0.3056	14.5449	0.1769	11.4376	0.9327
PCA	6.2581	0.3103	7.4447	0.2567	12.2954	0.9314
Sparse FI	2.3914	**0.9510**	3.8574	0.0418	21.1052	0.9361
GLP	2.5533	0.9479	3.8987	0.1919	22.4172	0.8249
Wavelet	2.5380	0.9224	3.7266	0.1249	20.1223	0.7242
UNB-PanSharp	7.2150	0.1758	15.6290	0.2039	10.4422	0.9328
GS	6.2373	0.3157	18.7107	0.2165	9.7761	**0.9415**
Proposed	**2.3571**	0.9422	**3.1774**	**0.0082**	**22.7498**	0.9353

TABLE III
QUALITY METRIC IN DATASET III

	ERGAS	CC	SAM	SID	PSNR	sCC
Best Values	0	1	0	0	$+\infty$	1
IHS	4.7097	0.7641	19.7087	0.4836	14.5437	0.9858
AIHS	4.6007	0.7671	12.6096	0.5797	14.3907	0.9878
PCA	7.1048	0.6381	40.6550	0.1666	9.7668	0.9862
Sparse FI	2.8285	0.9284	7.9172	0.3700	20.7410	0.9825
GLP	2.0851	0.9597	7.0922	0.2305	23.2611	0.9839
Wavelet	1.8227	0.9616	5.6624	0.2057	24.7426	0.9883
UNB-PanSharp	2.9271	0.9123	8.4291	0.2573	19.4102	0.9839
GS	4.7960	0.7769	24.2953	0.1317	13.4308	0.8890
Proposed	**2.0547**	**0.9638**	**4.2710**	**0.0960**	**23.6716**	**0.9952**

TABLE IV
QUALITY METRIC IN DATASET IV

	ERGAS	CC	SAM	SID	PSNR	sCC
Best Values	0	1	0	0	$+\infty$	1
IHS	5.5503	0.4364	10.0813	0.3384	12.8398	0.9936
AIHS	5.6546	0.4008	9.6739	0.3322	12.6237	0.9925
PCA	6.1342	0.4358	16.9040	0.2265	11.4973	0.9917
Sparse FI	2.9876	0.9034	5.6229	0.1965	18.1901	0.8720
GLP	2.7208	0.9139	4.9658	0.1779	19.0438	0.9904
Wavelet	2.3956	0.9083	5.4390	0.1842	18.1697	0.9922
UNB-PanSharp	3.0209	0.8297	8.3645	0.0658	16.5747	0.9932
GS	2.6036	0.8774	5.2805	0.0718	17.8756	0.9947
Proposed	**2.2322**	**0.9177**	**4.6021**	**0.0540**	**20.7629**	**0.9963**

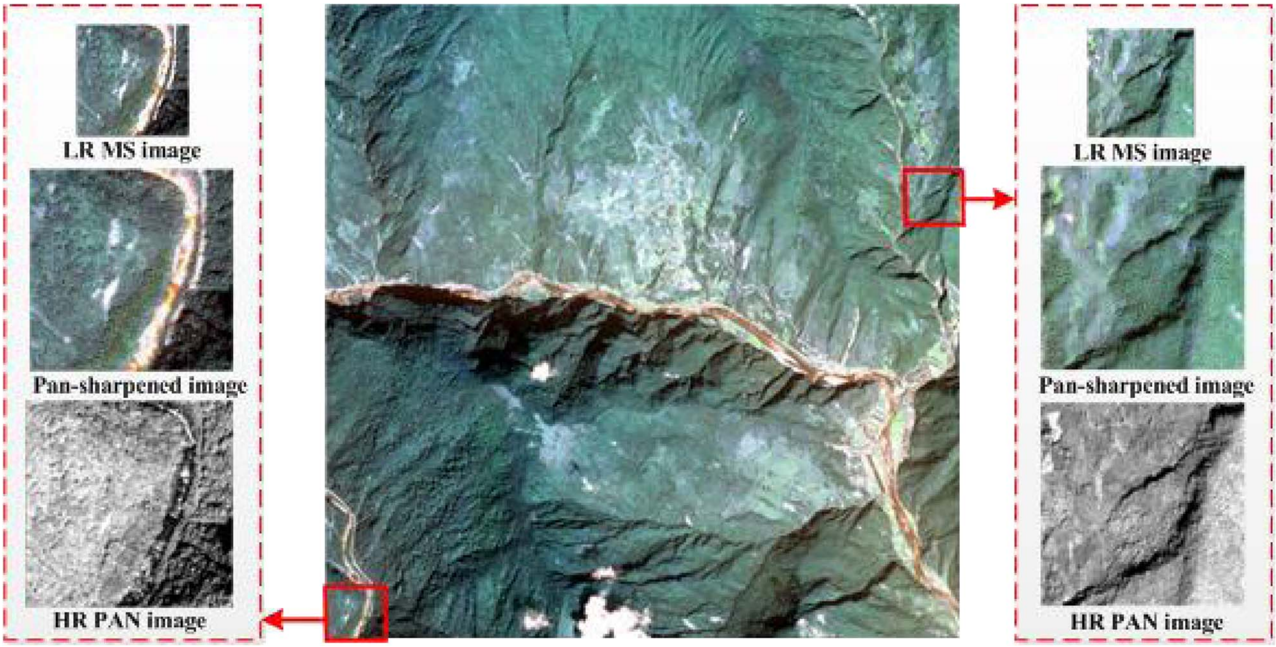

Fig. 14. Pan-sharpened IKONOS image by the proposed method.

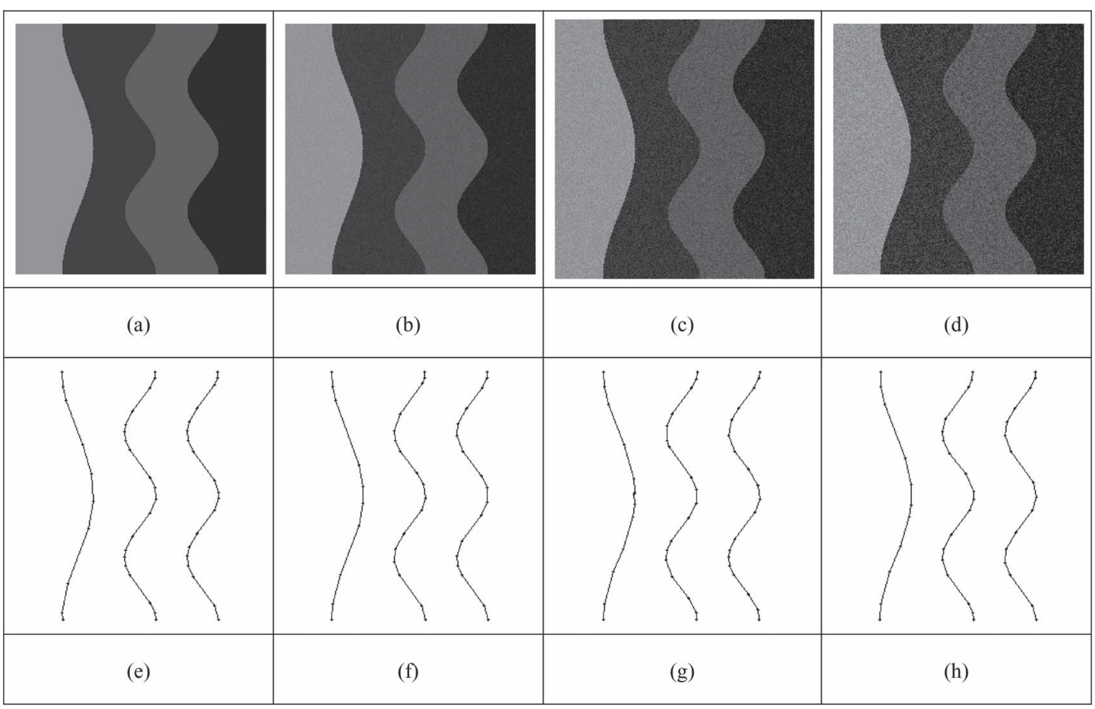

Fig. 15. Primal Sketch graph for synthetic image under different noisy conditions. (a) Original image with on noise. (b) Gauss noisy image with variance value as 5. (c) Gauss noisy image with variance value as 10. (d) Gauss noisy image with variance value as 15. (e) Primal Sketch obtained from the image (a). (f) Primal Sketch obtained from the image (b). (g) Primal Sketch obtained from the image (c). (h) Primal Sketch obtained from the image (d).

information. The proposed algorithm can get best values in most quality metrics. This can verify that the proposed learning interpolation algorithm for Pan-sharpening can achieve better results than other methods do.

To further verify improve the effectiveness of the proposed algorithm, the larger IKONOS LR MS and HR PAN images are shown in Fig. 14. The size of the LR MS image is 1000×1000, and the size of the HR PAN image is 4000×4000. The left and the right dashed box are the detail images for the red box parts. The whole Pan-sharpened image has better spectral information, and meanwhile, the spatial resolution is improved well.

C. Robustness for the Regional Map Under the Noisy Condition

The regional map is obtained according the Primal Sketch graph; hence, this experiment is to show the robustness for the

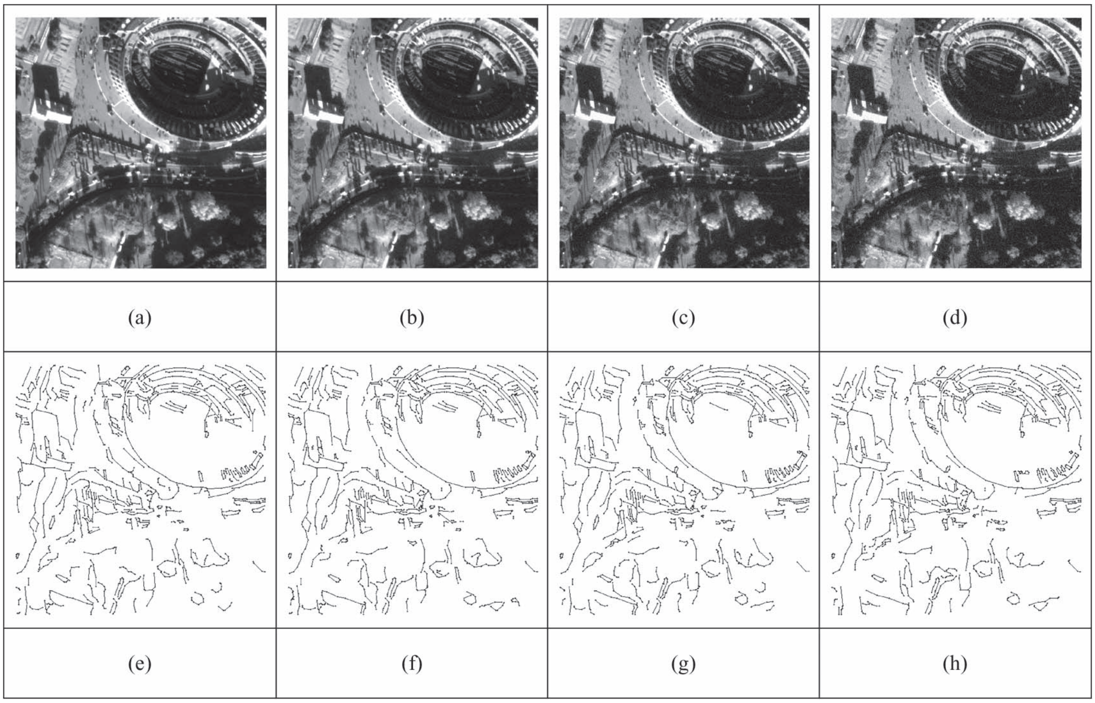

Fig. 16. Primal Sketch graph for HR PAN image under different noisy conditions. (a) Original image with no noise. (b) Gauss noisy image with variance value as 5. (c) Gauss noisy image with variance value as 10. (d) Gauss noisy image with variance value as 15. (e) Primal Sketch obtained from the image (a). (f) Primal Sketch obtained from the image (b). (g) Primal Sketch obtained from the image (c). (h) Primal Sketch obtained from the image (d).

Primal Sketch graph under the noisy condition. According to the steps for the Primal Sketch graph described in Section III, an analysis can be concluded that the initial sketch graph is similar to the canny edge detection algorithm, but not exactly the same. The filter used in the canny edge detection algorithm is only a subset of the primitives dictionary. As we all know, the canny edge detection algorithm has a better detection result when the noise in the image is additive noise. The filtering process is contained in the detection process to suppress the noise. In our paper, the Primal Sketch graph is obtained from the HR PAN image, under the most conditions, the noise is very moderate, and the noise is additive, hence the Primal Sketch graph is not affected when the noise is in the moderate levels.

Figs. 15 and 16 shows some experiments for verifying the correctness of the explanation. A synthetic image and a real HR PAN image are used as the test images. The noise added in the test image is Gauss noise with different variance values as 0, 5, 10, and 15. The noise in the HR PAN image is very moderate, and cannot be larger than 5 in variance value. From the results of the Primal Sketch graph, we can see that the Primal Sketch graph changes very little in different variance values. Particularly for the variance value that is less than 5, the Primal Sketch graphs are almost the same. Hence, in our proposed Pan-sharpening algorithm, the moderate noise cannot affect the accuracy of the regional division.

V. Concluding Remarks

The new algorithm of Pan-sharpening via learning interpolation is proposed in this paper. It is noted in this section that the HR PAN image is not injected into LR MS image to obtain the result. Combined with sketch information and regional maps, a fast-learning interpolation algorithm is designed to better keep spectral information. According to the gradient prior offered by an HR PAN image, the spatial resolution is effectively enhanced. It is proved by several groups of experiments that the proposed method can better balance the spectral information and spatial resolution. This is a new way for Pan-Sharpening the image, and it is very suitable for the images that have great differences in spectral information. The main disadvantage of the proposed Pan-sharpening algorithm consists of two parts: the imaging quality and the effectiveness of the noise. The proposed Pan-sharpening algorithm is based the spatial domain, and the computation for the adjustment parameter is dependent on the gradient of the HR PAN image. Hence, the imaging quality has some limitations to the proposed method. The imaging process is constrained in many ways, such as the atmospheric environment, or the imaging forming apparatus. Hence, before the Pan-sharpening process, some image preprocessing processes are necessary, such as image correction, image denoising, and image registration. When the image preprocessing is poor, or the preprocessing process is not ideal, the "spilling effect" in LR MS image, or the registration error may affect the Pan-sharpening results. Besides, the noise in the HR PAN image may affect the accuracy of the gradient calculation. When the noise is relatively small, this affect is not obvious, such as the test images in this paper. Moreover, the Primal Sketch graph and regional map are also not effect by the small noise. Better Pan-sharpening results can be obtained in our experimental results. However, when the noise is relatively large, some artifacts may appear in the

Pan-sharpened image. Hence, the proposed Pan-sharpening algorithm is suitable for the images with small noise. If the images have obvious noise, a denoising process is necessary before the Pan-sharpening process.

REFERENCES

[1] Z. Wang, D. Ziou, C. Armenakis, D. Li, and Q. Li, "Comparative analysis of image fusion methods," *IEEE Trans. Geosci. Remote Sens.*, vol. 43, no. 6, pp.1391–1402, Jun. 2005.

[2] P. Chavez, S. C. Sides, and J. A. Anderson, "Comparison of three different methods to merge multiresolution and multispectral data: Landsat TM and SPOT panchromatic," *Photogramm. Eng. Remote Sens.*, vol. 57, no. 3, pp. 311–316, Mar. 1991.

[3] M. Chikr El-Mezouar, N. Taleb, K. Kpalma, and J. Ronsin, "An HIS-based fusion for color distortion reduction and vegetation enhancement in IKONOS imagery," *IEEE Trans. Geosci. Remote Sens.*, vol. 49, no. 5, pp. 1590–1602, May 2011.

[4] Y. Zhang and G. Hong, "An HIS and wavelet integrated approach to improve pan-sharpening visual quality of natural colour IKONOS and QuickBird images," *Inf. Fusion*, vol. 6, no. 3, pp. 225–234, Sep. 2005.

[5] T. M. Tu, S. C. Su, H. C. Shyu, P. S. Huang, "A new look at HIS like image fusion methods," *Inf. Fusion*, vol. 2, no. 3, pp. 177–186, Sep. 2001.

[6] H. R. Shahdoosti and H. Ghassemian "Spatial PCA as a new method for image fusion," *Proc. 16th CSI AISP*, May 2012, pp. 090–094.

[7] C. A. Laben and B. V. Brower, Processing for enhancing the spatial resolution of multispectral imagery using pan-sharprning, U.S. Patent 6011875 A, Jan. 4 2000.

[8] S. Rahmani, M. Strait, D. Merkurjev, M. Moeller, and T. Wittman, "An adaptive HIS pan-sharpening method," *IEEE Geosci. Remote Sens. Lett.*, vol. 7, no. 4, pp. 746–750, Oct. 2010.

[9] C. Ballester, V. Caselles, L. Igual, J. Verdera, and B. Rouge, "A variational model for P+XS image fusion," *Int. J. Comput. Vis.*, vol. 69, no. 1, pp. 43–58, Aug. 2006.

[10] X. Otazu and M. Gonzalez-Ausicana, "Introduction of sensor spectral reponse into image fusion methods: Application to wavelet-based methods," *IEEE Trans. Geosci. Remote Sens.*, vol. 43, no. 10, pp. 2376–2385, Oct. 2005.

[11] A. Garzeli, F. Nencini, L. Alparone, and S. Baronti, "Multiresolution fusion of multispectral and panchromatic images through the curvelet transform," *Proc. IEEE IGARSS*, Jul. 2005, vol. 4, pp. 2838–2841.

[12] X. Qu, J. Yan, G. Xie, Z. Zhu, and B. Chen, "A novel image fusion algorithm based on bandelet transform" *Chin. Opt. Lett.*, vol. 5, no. 10, pp. 569–572, Oct. 2007.

[13] S. Y. Yang, M. Wang, L. C. Jiao, R Wu, and Z Wang, "Image fusion based on a new contourlet packet." *Inf. Fusion*, vol. 11, no. 2, pp. 78–84, Apr. 2010.

[14] V. P. Shah, N. H. Younan, and R. L. King, "An efficient pan-sharpening method via a combined adaptive PCA approach and contourlets," *IEEE Trans. Geosci. Remote Sens.*, vol. 46, no. 5, pp. 1323–1335, May 2008.

[15] S. Li and B. Yang, "A new pan-sharpening method using a compressed sensing technique," *IEEE Trans. Geosci. Remote Sens.*, vol. 49, no. 2, pp. 738–746, Feb. 2011.

[16] X. X. Zhu and R. Bamler, "A sparse image fusion algorithm with application to pan-sharpening," *IEEE Trans. Geosci. Remote Sens.*, vol. 51, no. 5, pp. 2827–2836, May 2013.

[17] T. Blu, P. Thevenaz, and M. Unser, "Linear interpolation revitalized," *IEEE Trans. Image Process.*, vol. 1, no. 3, pp. 710–719, May 2004.

[18] H. Hou and H. Andrews, "Cubic splines for image interpolation and digital filtering," *IEEE Trans. Acoust., Speech Signal Process.*, vol. 26, no. 2, pp. 508–517, Dec. 1978.

[19] T. M. Lehmann, C. Gonner, and K. Spitzer, "Addendum: B-spline interpolation in medical image processing," *IEEE Trans. Med. Imag.*, vol. 20, no. 7, pp. 660–665, Jul. 2001.

[20] L. Zhang and X. Wu, "An edge-guided image interpolation algorithm via directional filtering and data fusion," *IEEE Trans. Image Process.*, vol. 15, no. 8, pp. 2226–2238, Aug. 2006.

[21] K. Jensen and D. Anastassiou, "Subpixel edge localization and the interpolation of still images," *IEEE Trans. Image Process.*, vol. 4, no. 3, pp. 285–295, Mar. 1995.

[22] D. Zhou, X. Shen, and W. Dong, "Image zooming using directional cubic convolution interpolation," *IET Image Process.*, vol. 6, no. 6, pp. 627–634, Aug. 2012.

[23] A. Giachetti and N. Asuni, "Real time artifact-free image upscaling," *IEEE Trans. Image Process.*, vol. 20, no. 10, pp. 2760–2768, Oct. 2011.

[24] X. Li and M. T. Orchard, "New edge-directed interpolation," *IEEE Trans. Image Process.*, vol. 10, no. 10, pp. 1521–1527, Oct. 2001.

[25] D. Marr, *Vision*, New York, NY, USA: Freeman, 1982.

[26] S. C. Zhu, C. E. Guo, Y. Wang, and W. Xu, "What are textons?" *Int. J. Comput. Vis.*, vol. 62, no. 1, pp. 121–143, Apr./May 2005.

[27] W. Hu, H. Gong, S. C. Zhu, and Y. Wang, "An integrated background model for video surveillance based on Primal Sketch and 3D scene geometry," *Proc. IEEE Conf. Comput. Vis. Pattern Recognit.*, Jun. 2008. pp. 1–8.

[28] A. Buades, B. Coll, and J. M. Morel, "A non-local algorithm for image denoising," *Proc. IEEE Comput. Soc. Conf. Comput. Vis. Pattern Recognit.*, Jun. 2005,vol. 2, pp. 60–65.

[29] A. Buades, B. Coll, and J. M. Morel, "On image denoising methods," Tech. Note, CMLA, Cachan, France, 2004.

[30] Y. L. Liu, J. Wang, X. Chen, G. Yanwen, and Q. Peng, "A robust and fast non-local means algorithm for image denoising," *J. Comput. Sci. Technol.*, vol. 23, no. 2, pp. 270–279, Mar. 2008.

[31] X. Zhang, X. Feng, and W. Wang, "Two-direction non-local model for image denoising," *IEEE Trans. Image Process.*, vol. 22, no. 1, pp. 408–412, Jan. 2013.

[32] C. H. Lin, P. H. Tsai, K. H. Lai, and J. Y. Chen, "Cloud removal from multitemporal satellite images using information cloning," *IEEE Trans. Geosci. Remote Sens.* , vol. 51, no. 1, pp. 232–241, Jan. 2013.

[33] T. Ranchin and L. Wald, "Fusion of high spatial and spectral resolution images: The ARSIS concept and its implementation," *Photogramm. Eng. Remote Sens.*, vol. 66, no. 1, pp. 49–61, 2000.

[34] S. Chen, H. Su, R. Zhang, "The tradeoff analysis for remote sensing imagefusion using expanded spectral angle mapper," *Sensors*, vol. 8, no. 1, pp. 520–528, Sep. 2005.

[35] J. Saeedi and K. Faez, "A new pan-sharpening method using multiobjective partical swarm optimization and the shiftable contourlet transform," *ISPRS J. Photogramm. Remote Sens.*. vol. 66, no. 3, pp. 365–381, May 2011.

[36] B. Aiazzi, L. Alparone, F. Argenti, and S. Baronti "Wavelet and pyramid techniques for multisensor data fusion: A performance comparison varying with scale ratios," *Remote Sens. Int. Soc. Opt. Photon.*, vol. 3871, pp. 251–262, 1999.

[37] Zhang, Yun, and R. K. Mishra. "From UNB PanSharp to Fuze Go-the success behind the pan-sharpening algorithm," *Int. J. Image Data Fusion*. vol. 3, no. 1, pp. 39–53, 2014.

Cheng Shi received the bachelor's degree from the Xi'an University of Architecture and Technology, Xi'an, China. She is currently working toward the Ph.D. degree in computer application technology at Xidian University, Xi'an.

Her main research interests include multiscale geometric analysis, image processing, and information fusion.

Fang Liu (M'07–SM'07) received the B.S. degree in computer science and technology from Xi'an Jiaotong University, Xi'an, China, in 1984 and the M.S. degree in computer science and technology from Xidian University, Xi'an, in 1995.

She is currently a Professor with the School of Computer Science, Xidian University. She is the author or coauthor of five books and more than 80 papers in journals and conferences. Her research interests include signal and image processing, synthetic aperture radar image processing, multiscale geometry analysis, learning theory and algorithms, optimization problems, and data mining.

Lingling Li received the B.S. degree from the School of Electronic Engineering, Xidian University, Xi'an, China, where she is currently working toward the Ph.D. degree in the School of Electronic Engineering, Xidian University.

Her current research interests include community detection in networks and multiobjective optimization.

Licheng Jiao (SM'89) received the B.S. degree from Shanghai Jiaotong University, Shanghai, China, in 1982, and the M.S. and Ph.D. degrees from Xi'an Jiaotong University, Xi'an, China, in 1984 and 1990, respectively.

He is currently a Distinguished Professor with the School of Electronic Engineering, Xidian University, Xi'an. He has led approximately 40 important scientific research projects and has published more than ten monographs and 100 papers in international journals and conferences. He is the author of three books: *Theory of Neural Network Systems* (Xidian University Press, 1990), *Theory and Application on Nonlinear Transformation Functions* (Xidian University Press, 1992), and *Applications and Implementations of Neural Networks* (Xidian University Press, 1996). He is the author or coauthor of more than 150 scientific papers. His research interests include signal and image processing, natural computation, and intelligent information processing.

Prof. Jiao is a member of the IEEE Xi'an Section Executive Committee and the Chairman of the Awards and Recognition Committee and an executive committee member of the Chinese Association of Artificial Intelligence.

Yiping Duan received the B.S. degree from the School of Computer, Henan Normal University, Henan, China. She is currently working toward the Ph.D. degree in the School of Computer, Xidian University, Xi'an, China.

Her current research interests include semantic mining, machine learning, and synthetic aperture radar image processing.

Shuang Wang (M'07) was born in Shannxi, China, in 1978. She received the B.S., M.S., and Ph.D. degrees from Xidian University, Xi'an, China, in 2000, 2003, and 2007, respectively, all in circuits and systems.

She is currently a Professor with the Key Laboratory of Intelligent Perception and Image Understanding of the Ministry of Education of China, Xidian University. Her main research interests are image processing, machine learning, synthetic aperture radar (SAR), polarimetric SAR image processing, etc.

Learning Interpolation via Regional Map for Pan-Sharpening

Cheng Shi, Fang Liu, *Senior Member, IEEE*, Lingling Li, Licheng Jiao, *Senior Member, IEEE*, Yiping Duan, and Shuang Wang, *Member, IEEE*

***Abstract*—Although the bandwidth of the high-resolution panchromatic (HR PAN) image is wide, it is narrow in each band of the low-resolution multispectral (LR MS) image. Hence, the spatial resolution of the HR PAN image is much higher than that of the LR MS image. However, HR PAN image only has a single band. The purpose of the Pan-sharpening algorithm is to make the Pan-sharpened image with both high spatial resolution and good spectral information. In this paper, a novel learning interpolation method for Pan-sharpening is proposed by expanding the sketch information in the HR PAN image. The sketch information contains the edges and lines features of the image, and each segment of the sketch information has its own direction. According to the primal sketch graph of the HR PAN image, a regional map is obtained by a designed geometrical template. Since the size of the HR PAN image is different from that of the LR MS image, the LR MS image is interpolated into an interpolated multispectral (IMS) image by the nearest interpolation method. In addition, the IMS image can be mapped into the structure and the nonstructure regions by this regional map. The nonstructure regions are divided into the smooth and the texture regions by a variance value. For the structure and texture regions, the interpolated pixels in the IMS image are relearned and readjusted by the proposed structure and texture learning interpolation method, respectively. Experimental results show that the proposed Pan-sharpening method can provide superior performance in both visual effect and quality metrics, particularly for the images with a large spectral difference.**

***Index Terms*—Learning interpolation, pan-sharpening, primal sketch, regional map.**

Manuscript received November 7, 2013; revised March 3, 2014 and September 13, 2014; accepted November 17, 2014. The work was supported in part by the National Basic Research Program (973 Program) of China under Grant 2013CB329402; by the National Natural Science Foundation of China under Grant 61173090, Grant 61173092, Grant 61271302, and Grant 61272282; by the National Research Foundation for the Doctoral Program of Higher Education of China under Grant 20110203110006; by the Fund for Foreign Scholars in University Research and Teaching Programs (the 111 Project) under Grant B07048); by the Program for Cheung Kong Scholars and Innovative Research Team in University under Grant IRT1170; by the Fundamental Research Funds for the Central Universities under Grant JB140317; and by the EU FP7 IRSES Grant under Grant 247619 on "Nature Inspired Computation and its Applications (NICaiA)."

C. Shi, F. Liu, and Y. Duan are with the School of Computer Science and Technology, Xidian University, Xi'an 710071, China, the Key Laboratory of Intelligent Perception and Image Understanding of Ministry of Education, Xi'an 710071, China, and also with the International Research Center for Intelligent Perception and Computation, Xidian University, Xi'an 710071, China (e-mail: f63liu@163.com).

L. Li, L. Jiao, and S. Wang are with the Key Laboratory of Intelligent Perception and Image Understanding of Ministry of Education, Xi'an 710071, China and also with the International Research Center for Intelligent Perception and Computation, Xidian University, Xi'an 710071, China.

Color versions of one or more of the figures in this paper are available online at http://ieeexplore.ieee.org.

Digital Object Identifier 10.1109/TGRS.2014.2375931

I. Introduction

IMAGE fusion refers to the process of combining images from different sensors. If the images to be fused include the low-resolution multispectral(LR MS) image and the high-resolution panchromatic (HR PAN) image, the fusion process is called "Pan-Sharpening" [1], [2].

In the past several years, many Pan-Sharpening methods are present. The classical Pan-Sharpening methods are IHS (Intensity, Hue, and Saturation) [3], [4], PCA (Principal Component Analysis) [5], [6], Gram–Schmidt [7], and Brovery *et al.* [5] transform These methods can improve the spatial effectively information but spectral distortion often appears. To overcome this problem, some popular Pan-sharpening methods are proposed, such as adaptive IHS [8], P+XS [9], wavelet-based method [10], and multiscale geometric analysis (MGA)-based method [11]–[14]. Some MGA tools are widely used in the Pan-Sharpening process, such as Curvelet [11], Bandlet [12], and Contourlet *et al*. [13], [14]. These tools can maintain spectral information better than the classical methods; however, it is impossible for the MGA tools to represent the directions adaptively, which make the balance in spatial resolution difficult.

Recently, the sparse-based method has been gradually studied [15], [16]. Compared with the classical and the optimized Pan-Sharpening algorithm, the proposed Pan-Sharpening results depend on the corrections between the HR PAN image and the injected image. Compared with these methods, the difference of the sparse-based method is that the HR PAN image is not injected into the LR MS image directly (both in the spatial and the frequency domain). The sparse-based method establishes a relationship between the low- and high-resolution images by training a dictionary on a training set, and then according to this relationship, the information of the low-resolution image is used to get its high-resolution version. The sparse-based method gives us a new way for Pan-Sharpening process-improve, but not inject. In this kind of method, the dictionary training is very important. In the method proposed by Li and Yang [15], the dictionary training set was constructed by training the high-resolution MS (HR MS) image and its downsampled image (the low-resolution MS images). However, for a true sensor, the HR MS image (the same resolution with HR PAN image) is impossible to obtain. Zhu and Bamler [16] improved Li's method, the HR PAN and the downsampled LR PAN images are used to train the dictionary. A better Pan-Sharpening result can be obtained for the images with a continuous boundary, but for discontinuous images (images that have rapid changes in details), the detail loss always appears. Thus, the sparse-based method is more suitable for the image with many continuous lines.

"Super-resolution"-based method is based on the LR MS image to get the high-resolution MS image; hence, it can better maintain the spectral information in the Pan-Sharpened image. Meanwhile, the Pan-sharpened result depends on whether the dictionary can better represent the image information or not. In order to overcome the dependence of Pan-Sharpened results on dictionary training and the disadvantage in representing the detail information, the learning interpolation-based Pan-sharpening method is proposed.

Interpolation methods mainly consist of two kinds: the linear-based method and the edge direction-based method. Typical linear interpolation methods include nearest neighbor interpolation, linear interpolation, cubic interpolation, and B-spline interpolation, etc. [17]–[19]. These interpolation methods are simple, but the diffusion phenomenon always appears. Hence, some edge direction-based methods are proposed [20]–[24]. Jensen and Anastassiou [21] gave an edge-directed interpolation method, and Zhou *et al.* [22] proposed an directional cubic convolution interpolation method. These two methods have more complex models, and meanwhile, the interpolation results are affected by the accuracy of edge detection. Giachetti and Asuni [23] proposed an iterative curvature-based interpolation (ICBI) method for real-time applications, and it is suitable for the curvature continuity, curvature enhancement, and isophote contour, but the parameter selection has a great effect on the results. A new edge-directed interpolation (NEDI) method, proposed by Li [24], uses the statistical property of covariance on the edge of the image, and better maintains edge information in the interpolated image. NEDI method has a simple linear prediction model, and does not require the edge detection process.

These interpolation algorithms can maintain better spectral information in the interpolated image, however they are just suitable for continuous lines. In the Pan-sharpening problem, the existence of many discontinuous lines makes it hard to get an ideal spatial resolution in these interpolation methods. Thus a learning interpolation method for Pan-sharpening is proposed. Combine the computer visual model and the Non-local theory, under the guidance of the HR PAN image, the LR MS image is interpolated into the Pan-sharpened image.

This paper is structured as follows. In Section II, the related work is presented. Section III shows the proposed Pan-sharpening algorithm. Experimental results and parameter analysis is done in Section IV. Finally, we conclude a brief summary in Section V.

II. Related Work

Consider the following interpolation model (assume the size of the high-resolution image is two times that of the low-resolution image):

$$f_{HR}(2i+1, 2j+1) = \sum_{k=0}^{1}\sum_{l=0}^{1} \alpha_{2k+l} f_{HR}\left(2(i+k), 2(j+l)\right) \quad (1)$$

where f_{LR} (with size $W \times H$) is a low-resolution image, and f_{HR} (with size $2W \times 2H$)is the high-resolution image of f_{LR}, such as $f_{HR}(2i, 2j) = f_{LR}(i, j)$ $(i = 1, \ldots, W,\ j = 1, \ldots, H)$.

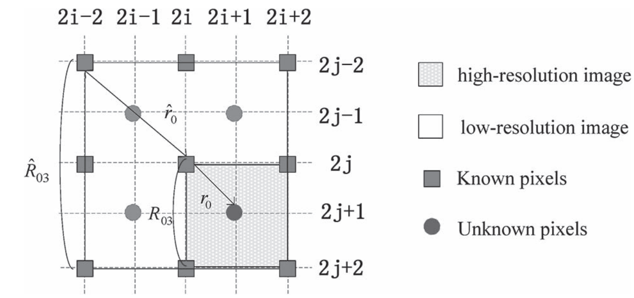

Fig. 1. Geometric regularity for low- and high-resolution images.

$\vec{\alpha} = \alpha_{2k+l}|_{\substack{k=0,1\\ l=0,1}} = (\alpha_0, \alpha_1, \alpha_2, \alpha_3)^T$ represents the weight vector. Equation (1) is used to estimate the pixel values $f_{HR}(2i+1, 2j+1)$ by weighting its four neighborhood pixels that come from the low-resolution image. The NEDI method consists of two steps, the first step is to estimate the pixels $f_{HR}(2i+1, 2j+1)$, and the second one is to estimate the pixels $f_{HR}(2i+1, 2j)$ and $f_{HR}(2i, 2j+1)$. In the first step, the pixels at position $(2i, 2j)$ are called "known pixels" in this paper, and the other pixels are called "unknown pixels." Moreover, in the second step, the pixels at position $(2i, 2j)$ and $(2i+1, 2j+1)$ are called "known pixels," and the other pixels are called "unknown pixels." In the following, we will describe the calculation of $f_{HR}(2i+1, 2j+1)$.

The problem now is how to compute the weight $\vec{\alpha}$, that is, to say how to estimate the pixel $f_{HR}(2i+1, 2j+1)$. The weight $\vec{\alpha}$ plays an important role in the interpolation process. NEDI method is proposed by Li and Orchard[24]. It uses the statistical property of the edge information and the geometric duality of the low- and high-resolution images. Only the low-resolution image is used to estimate the high-resolution image. The interpolation process is adaptive, and it has great advantages in interpolating images with continual edges. Now, the weight computation in the NEDI method is described as follows.

According to the classical Wiener filter theory, the optimal MMSE linear interpolation coefficients can be presented as

$$\vec{\alpha} = R^{-1}\vec{r} \quad (2)$$

where $\vec{\alpha}$ is a weight vector, and R is a covariance matrix of the four-order neighborhood of $f_{HR}(2i+1, 2j+1)$. $[R_{kl}](0 \le k, l \le 3)$ contains 16 values, and $\vec{r}$ is the cross-covariance matrix, which contains four elements. For example, $R_{03} = E[f_{HR}(2i, 2j), f_{HR}(2i, 2j+2)]$, and $r_0 = E[f_{HR}(2i, 2j), f_{HR}(2i+1, 2j+1)]$.

According to (2), the weight $\vec{\alpha}$ can be obtained. However, the problem is that $f_{HR}(2i+1, 2j+1)$ is an unknown pixel. In this case, how can we know the high-resolution covariance when we only have a low-resolution image? In [24], Li and Orchard considered that the edges of the high- and the low-resolution images have a property called "geometric regularity." We can replace the value of R and r in the high-resolution image by the $\hat{R}$ and $\hat{r}$ in the low-resolution image. The computation process of $\hat{R}$ and $\hat{r}$ is shown in Fig. 1. According to

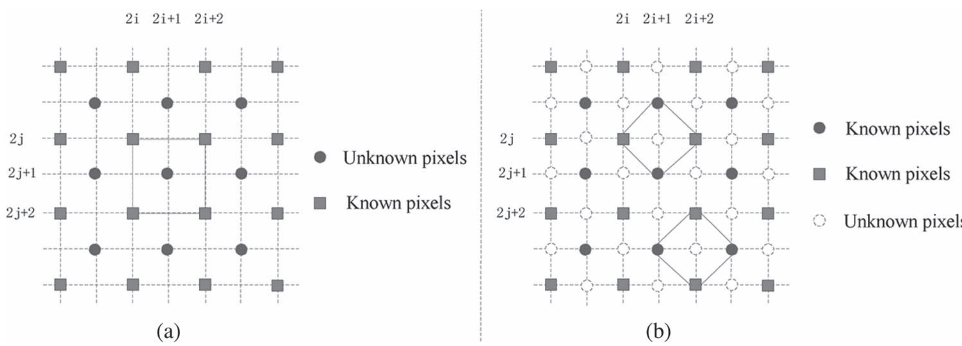

Fig. 2. Interpolation process by NEDI [(a) and (b) are the high-resolution images]. (a) First step for NEDI. (b) Second step for NEDI.

this property, the high-resolution covariance $\hat{R}$ and the cross-covariance matrix $\hat{r}$ can be obtained by the classical covariance method. Then, $\hat{R}$ and $\hat{r}$ can be calculated by

$$\hat{R} = \frac{1}{M^2}C^T C \quad \hat{\vec{r}} = \frac{1}{M^2}C^T \vec{y} \tag{3}$$

where $N \times N$ is the size of a local window used to train the weight. $\vec{y} = [y_1, y_2, \ldots, y_{\mathrm{M}^2}]^T$ is the known pixels in the window, C is a matrix with size $\mathrm{M}^2 \times 4$ (M is the number of the known pixels in the local window), and the kth row of C is the four neighborhood-known pixels of y_k. By training the weight for each known pixel in the local window, and according to (2) and (3), the weight $\vec{\alpha}$ can be calculated by

$$\vec{\alpha} = (C^T C)^{-1}(C^T \vec{y}). \tag{4}$$

Equation (1) shows how to estimate the pixel $f_{HR}(2i + 1, 2j + 1)$. The second step is to estimate the other unknown pixels ($f_{HR}(2i + 1, 2j)$ and $f_{HR}(2i, 2j + 1)$). There is a process similar to the aforementioned step. Rotate the training window by 45° to select the neighborhood pixels, and calculate the weight $\vec{\alpha}$ according to (4) (more details can be found in [24]). Fig. 2 shows the interpolation process of NEDI.

III. Learning Interpolation Based on Regional Map

NEDI can better maintain spectral information in the interpolated image, making it very suitable for the Pan-sharpening problem. However, all the interpolation algorithms are more suitable for the image with continuous boundary, but for the discontinuous edges, a minor change in the interpolated image may be ignored. Hence, it cannot satisfy the spatial resolution requirement in the Pan-sharpening problem. In the Pan-sharpening problem, minor details are also important to the following processing. To construct the interpolated image more precisely, the learning interpolation model is designed and shown in (5)

$$f_{HR}(2i{+}1, 2j{+}1) {=} \sum_{k=0}^{1}\sum_{l=0}^{1} \alpha_{2k+l} f_{HR}\left(2(i{+}k), 2(j{+}l)\right) + \delta(2i + 1, 2j + 1). \tag{5}$$

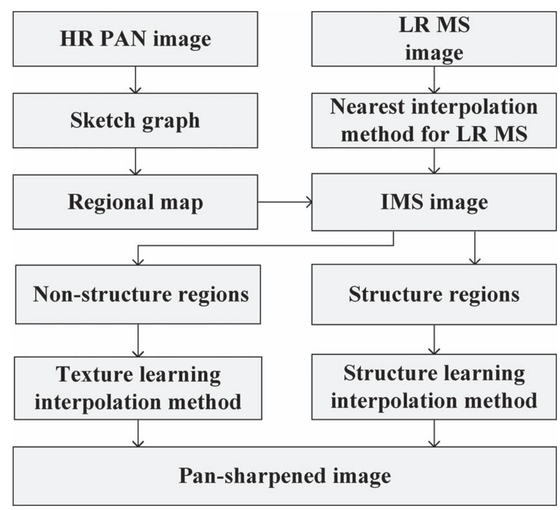

Fig. 3. Block diagram of learning interpolation via regional map for Pan-sharpening (Assume the size of the HR PAN image is two times larger than the LR MS image).

Equation (5) is an improvement of (1). f_{HR} is the Pan-sharpened HR MS image, and δ is an adjustment parameter, which reflects the difference between the Pan-sharpened HR MS image and the predicted interpolated image (the image is interpolated only by weight parameter α_{2k+l}). Similar to NEDI, the learning interpolation model consists of two steps, the first step is to estimate the pixel $f_{HR}(2i + 1, 2j + 1)$, and the second step is to estimate $f_{HR}(2i + 1, 2j)$ and $f_{HR}(2i, 2j + 1)$. For each step, the learning interpolation consists of three parts: regional division, the weight parameter estimation, adjustment of the learning interpolation pixels under the guidance of HR PAN image. The learning interpolation algorithm can only enlarge the low-resolution image twice. Hence, in the sections of regional division, weight learning, and adjustment parameter learning, we assume that the size of the HR PAN image is two times that of the LR MS image. The block diagram of the learning interpolation is shown in Fig. 3. In the following sections, we describe each part in detail.

A. *Regional Division for IMS Image According to the Regional Map of HR PAN Image*

Marr proposed the concept of "primal sketch" [25]. He thought that the image can be divided into two components, "sketchable" and " nonsketchable" parts. The "sketchable" part

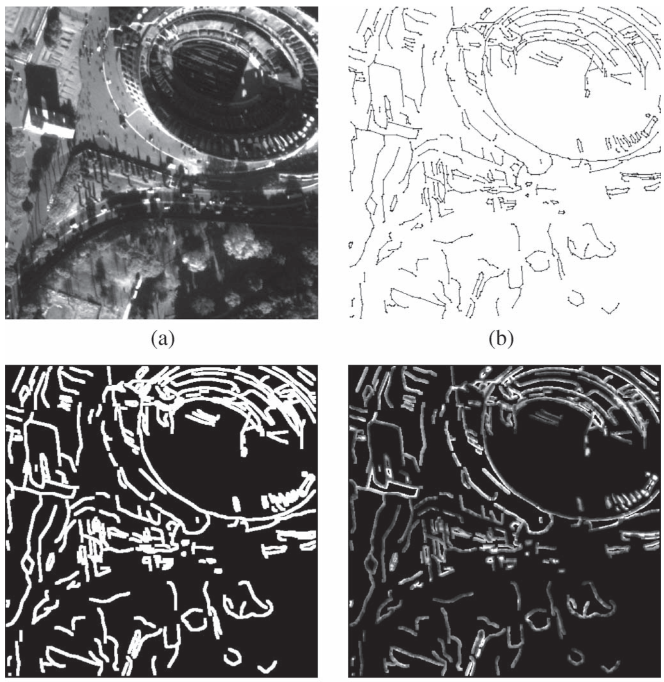

(a) (b)

(c) (d)

Fig. 4. Sketch graph and structure division. (a) Original HR PAN image. (b) Sketch graph. (c) Regional map (concept-map, which reflects the regions where the lines and edges lie in. The white region is the structure region, and the black region is the nonstructure region, and the size of the template is 7×7). (d) Extracted structure regions of (a) (The structure regions are mapped into the original image, and nonstructure regions are marked as black color).

just contains the structure of the image, and the " nonsketchable" part contains the texture and smooth regions. People always focus on the primal sketch of the image, for it contains the key information about the image sense. Marr has done a lot of objective description for primal sketch, but no explicit mathematical model was given. In 2003, Zhu gave a theoretical model of the primal sketch in the International Computer Vision Conference [26], [27], which is different from the traditional edge detection algorithm; the sketch graph is constructed by the segments with directions. The main steps are shown as follows.

1. Take the convolution operations on the input image by the Gauss-order differential filter and Gaussian second-order differential filter, respectively.
2. Fuse the filtered images to obtain the energy diagram, which reflects the brightness variations of the image.
3. Obtain an initial sketch graph by using the nonmaxima suppression algorithm on the energy diagram.
4. The final Primal Sketch graph can be obtained by the greedy pursuit algorithm and a group of graph operators.

Fig. 4(b) shows the sketch graph of the HR PAN image. The segment in the sketch graph only has a single pixel; however, the edges of the image have a certain width. Therefore, along the direction of each segment, a template is designed to represent the geometric structure block of the image. The pixels in the same line have the same direction, and each pixel in one geometric structure block has the same direction.

(a) (b)

Fig. 5. Designed template for constructing the regional map (a) Designed template in Sketch graph (The red window is the selected window with center at the green pixel). (b) Designed geometric template for the segment l (the block circle is represent the each pixel in the original image).

According to the designed template, the image can be divided into the structure and the nonstructure regions [see Fig. 4(d)]. The binary map of the structure and the nonstructure regions is called "regional map" in this paper. Fig. 5 shows the designed template and Fig. 4(c) gives the regional map.

The variance value reflects the statistical properties of the image. For the nonstructure regions, when the variance value is less than a certain threshold T, the region has small changes in gradient value, and then, we call it "smooth region"; otherwise, the region is called "texture region." Now, the image can be divided into the structure, texture, and smooth regions.

For the Pan-sharpening problem, the regional map and the variance calculation are obtained from the HR PAN image. Since the HR PAN image has a different size with the LR MS image, the LR MS image is first interpolated into an interpolated multispectral (IMS) image by the nearest interpolation method (copy the value of each pixel of the LR MS image to its neighborhood pixels to get the IMS image). The IMS image has the same size with HR PAN image. In addition, according to the regional map and the variance value obtained by HR PAN image, the IMS image is mapped into structure, texture, and smooth regions. In the following sections, the pixels in the position of $(2i+1, 2j+1)$, $(2i+1, 2j)$, and $(2i, 2j+1)$ in the IMS image will be reestimated to get a more accurate interpolated pixel.

B. Estimate the Weight Parameter

In the traditional NEDI algorithm, only the local window is used to compose the training set in the training process (the process aims to form the matrix C). However, the pixels in the local window may not have the similar structures. Hence, the error of the training set will lead to the calculation error of $\vec{\alpha}$. In order to estimate the weight parameter $\vec{\alpha}$ more precisely, the global information should be considered. The nonlocal idea has been successfully applied to image denoising [28]–[31]. It can maintain the edge and texture information better. This idea can also be applied to learning the interpolation weight. In our interpolation problem, these similar blocks should have a similar weight. Hence, all the blocks, similar to the interpolated

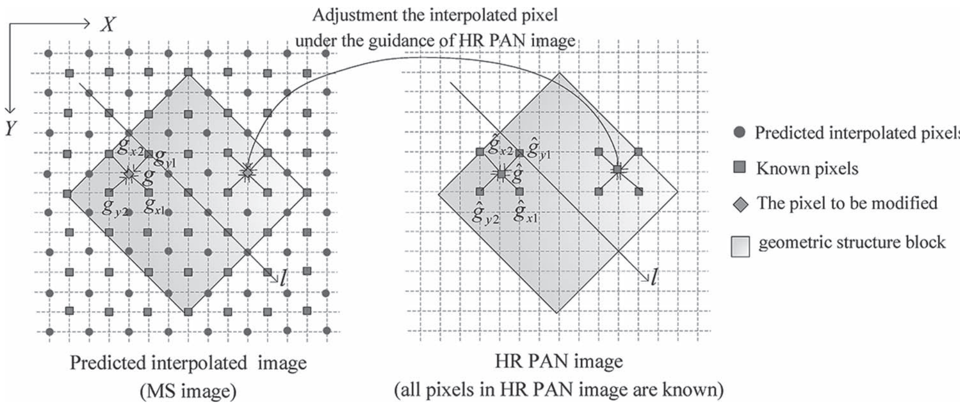

Fig. 6. Adjustment learning for the structure regions (l is the segment in the primal sketch graph).

pixel, are searched to form the matrix C (we call it "weight training set"), and then the weight is learned according to (4). Now, the problem to be solved is the high computational complexity of the nonlocal search. It is hard to achieve a real global search, and thus a fast global search algorithm based on the direction of the geometric structure block is proposed.

In section A, the IMS image can be divided into the structure, texture and smooth regions. Each segment has its direction in the structure region. Similar blocks should have a similar direction. If the interpolated pixel (the pixels in the position of $(2i+1, 2j+1)$ in the first step, or $(2i+1, 2j)$ and $(2i, 2j+1)$ in the second step) is in the structure regions, its directions can be considered as the direction of its four neighborhood-known pixels. Thus its similar blocks can be obtained by calculating the similarity with the same direction blocks. In addition, the weight can be learned according to these similar blocks. If the interpolated pixel is in the nonstructure regions, two cases should be considered. For the smooth region, the weight is $\vec{\alpha} = [0.25, 0.25, 0.25, 0.25]$, and for the texture region, the weight is estimated by the NEDI algorithm.

After learning the weight parameter $\vec{\alpha}$, the pixel to be reinterpolated in the IMS image can be estimated by linear weighting its four neighborhood pixels (similar process to NEDI). In the following sections, the linear weighted pixel is called "predicted interpolated pixel."

C. Adjustment of the Predicted Learning Interpolation Pixels Under the Guidance of HR PAN Image

The predicted interpolated image better maintains spectral information. However, the details may not be accurate, particularly for the minor details. To further improve the detail information in the Pan-sharpened image, it is necessary to make an adjustment parameter δ to the predicted interpolated pixel. The idea of the adjustment parameter learning comes from the Poisson equation-based image recovery. Lin *et al.* [32] proposed a cloud cloning algorithm in their paper. The basic idea is to clone information from cloud-free patches to their corresponding cloud-contaminated patches in several images (These images are obtained from different time, but for the same place). The cloud-contaminated patches can be recovered according to the gradient field provided by the cloud-free patches. Meanwhile, the boundary in the cloud-contaminated patches is unchanged. The boundary condition can maintain the spectral information of the cloud-contaminated image. The adjustment parameter δ cannot be obtained if we only have the LR MS image. However, in the Pan-sharpening problem, we have the HR PAN image that has a similar structure with the Pan-sharpened image. Thus, the gradient information of the HR PAN image is considered when estimating δ. The solution of the Poisson equation has high computational complexity, and in the proposed Pan-sharpening algorithm, only one interpolated pixel needs to be adjusted for each time. Therefore, the process can be simplified. The proposed method to estimate the adjustment parameter δ is to add δ to the predicted interpolated pixel, and make the predicted interpolated image of a similar gradient value with the HR PAN image. Hence, the adjust model is

$$\min_{\delta} \left\{ (f_x(\delta) - \lambda_1 \hat{f}_x)^2 + (f_y(\delta) - \lambda_2 \hat{f}_y)^2 \right\} \tag{6}$$

where f_x and f_y represent the gradient function calculated in the predicted interpolated image along the different directions. The variable of the function is the parameter δ. In addition, $\hat{f}_x$ and $\hat{f}_y$ mean the gradient value in the HR PAN image. λ_1 and λ_2 are the intensity parameters that determine the intensity of the adjustment. Too large of the values λ_1 and λ_2 will result in an artificial phenomenon in the Pan-sharpened image; however, too small of their values will lead to the image blur. Thus, the parameters λ_1 and λ_2 are set to adjust the gradient value of the HR PAN image. The parameters λ_1 and λ_2 are calculated in

$$\begin{aligned} \lambda_1 &= (g_{x1} - g_{x2})/(\hat{g}_{x1} - \hat{g}_{x2}) \\ \lambda_2 &= (g_{y1} - g_{y2})/(\hat{g}_{y1} - \hat{g}_{y2}) \end{aligned} \tag{7}$$

where g_{x1} and g_{x2} are the neighborhood-known pixels in the predicted interpolated image, which are searched along the gradient computation direction of f_x. $\hat{g}_{x1}$ and $\hat{g}_{x2}$ are the pixel values in the HR PAN image, which have the same position with g_{x1} and g_{x2}. If $\hat{g}_{x1} = \hat{g}_{x2}$, $\lambda_1 = 1$, and if $\hat{g}_{y1} = \hat{g}_{y2}$, $\lambda_2 = 1$. The positions of these four pixels are shown in Fig. 6.

Now, we describe the direction selection when calculating the gradient function f_x and f_y. By the regional map, the IMS image can be divided into the structure and the nonstructure regions. In the structure region, edge direction can be obtained by the direction of the geometric structure block. Along the edge direction, the changes in gray value are continuous, and perpendicular to the edge direction, the gradient is changed dramatically. The aim of computing parameter δ is to keep the continuous information along the edge direction, and modify the detail information perpendicular to the edge direction. Hence, for the structure region, f_x is calculated along the edge direction, and f_y is calculated perpendicular to the edge direction. The first term in (6) can be considered as the smooth term, and the second means the gradient modify term. The coordinate direction is shown in Fig. 6. In the texture region, f_x is calculated along the 45° in the first interpolation step, and 0° in the second step.

After determining the gradient computation directions, add the parameter δ to the predicted interpolated pixel, and obtain the gradient functions f_x and f_y, respectively. In addition, compute the gradient values $\hat{f}_x$ and $\hat{f}_y$ in the HR PAN image. f_x, f_y, $\hat{f}_x$, and $\hat{f}_y$ are calculated in

$$\begin{aligned} f_x(\delta) &= g_{x1} + g_{x2} - 2(g+\delta) \quad & \hat{f}_x &= \hat{g}_{x1} + \hat{g}_{x2} - 2\hat{g} \\ f_y(\delta) &= g_{y1} + g_{y2} - 2(g+\delta) \quad & \hat{f}_y &= \hat{g}_{y1} + \hat{g}_{y2} - 2\hat{g} \end{aligned} \tag{8}$$

where g is the predicted interpolated pixel in the IMS image, and $\hat{g}$ is the pixel in the HR PAN image, which has the same position with g. Equation (6) is a minimization problem, and each term in (6) is a quadratic function; hence, its solution can be easily derived by assuming the first-order derivative of the relative objective function equals to zero.

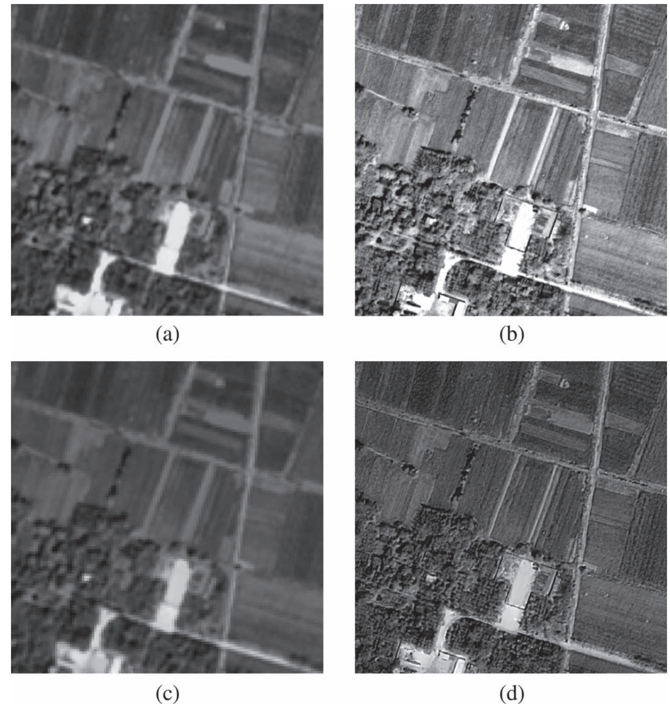

Fig. 7. Learning interpolation for the intensity component of the LR MS image. (a) LR MS image. (b) HR PAN image. (c) Intensity component of the LR MS image. (d) New intensity component after learning interpolation process.

D. Proposed Pan-Sharpening Algorithm-Based on Learning Interpolation and Regional Map

Using the sketch information of the HR PAN image, the regional map and geometric structure block are obtained. It is worth mentioning that the size of the HR PAN image is four times that of the LR MS image for most satellite images; hence, the aforementioned learning interpolation process should be repeated twice. For the first time, the regional map and the HR PAN image are obtained by downsampling the real regional map and original HR PAN image, respectively. For each interpolation process, it consists of two steps, and the first step is to estimate the pixel $f_{HR}(2i+1, 2j+1)$, and the second step is to estimate $f_{HR}(2i, 2j+1)$ and $f_{HR}(2i+1, 2j)$.

In the first step, the interpolated pixel value at position $(2i+1, 2j+1)$ is learned by the learning interpolation method. After the first step, more accurate pixel values at position $(2i+1, 2j+1)$ can be obtained. In the second step, the pixels $f_{HR}(2i, 2j+1)$ and $f_{HR}(2i+1, 2j)$ are estimated based on the result obtained in the first step. From Fig. 2(b), we can see that the second interpolation step is to rotate the training window by 45°. Repeat the learning process twice until all the pixels are interpolated.

The proposed Pan-sharpening algorithm makes full use of the advantage that the spectral information can be kept well before and after the LR MS image is interpolated. In addition, according to the adjustment process, high-resolution Pan-sharpened image can be obtained. Fig. 7 shows an example of modification process. Fig. 7(a) is the LR MS image, and Fig. 7(b) is the HR PAN image. Fig. 7(c) is the intensity component of the LR MS image (obtained by HIS transform). Fig. 7(d) is the modified image by the LIPM model. From Fig. 7(b) and (c), we can see that the HR PAN image has a great difference in spectral information compared with the LR MS image. If the intensity component is substituted by the HR PAN image (or the details of the PAN image) directly, significant distortion will appear in the Pan-Sharpened image. Fig. 7(d) has a better clarity; meanwhile, it has similar spectral information with Fig. 7(c). The block diagram is shown in Fig. 7.

IV. Performance Evaluation

The proposed method for Pan-Sharpening is evaluated in this section. A series of simulation experiments are done using the QuickBird, WorldView-II, and IKONOS images that are from the Internet (http://glcf.umd.edu/data/). Fig. 8 shows the original LR MS and the HR PAN images. The size of the LR MS image is 128 × 128, and the size of the HR PAN image is 512 × 512. For the QuickBird image, the resolution of the LR MS image is 2.44 m, and the resolution of the HR PAN image is 0.61 m. For the WorldView-II image, the size of the LR MS image and the HR PAN images are 2 and 0.5 m, respectively. For the IKONOS image, the size of the LR MS image and the HR PAN images are 4 and 1 m, respectively.

Many well-known quality metrics for spectral information and spatial resolution are used to evaluate the effective of the proposed Pan-sharpening algorithm.

- Quality metrics for spectral information: Relative dimensionless global error in synthesis (ERGAS) [33], correlation coefficient (CC), spectral angle mapper (SAM) [34],

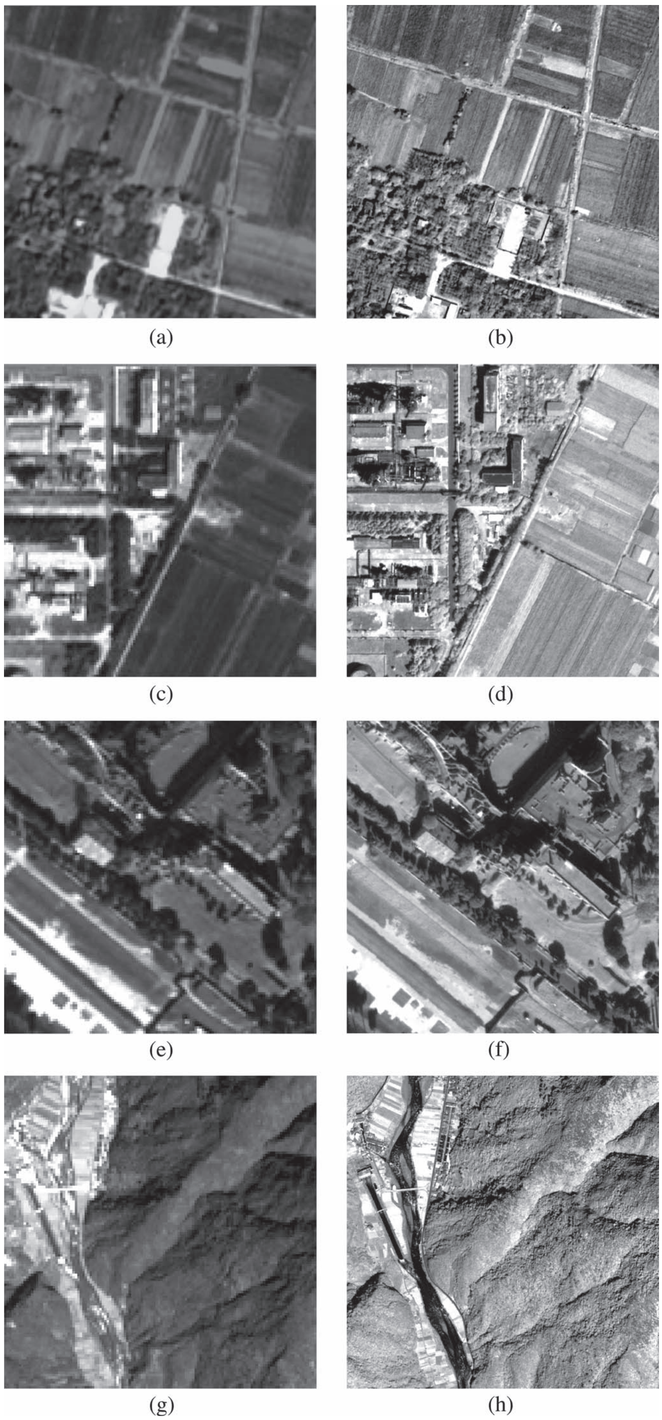

Fig. 8. Original LR MS and HR PAN image. (a) and (b) LR MS and HR PAN QuickBird image of dataset 1. (c) and (d) LR MS and HR PAN QuickBird image of dataset 2. (e) and (f) LR MS and HR PAN WordView-II image of dataset 3. (g) and (h) LR MS and HR PAN IKONOS image of dataset 4.

and spectral information divergence (SID) are used to evaluate the spectral quality.

- Quality metrics for spatial resolution: Peak signal-to-noise ratio (PSNR), and spatial CC (sCC, compare the CC for the high-frequency between the Pan-sharpened image and HR PAN image) [35]) are used to evaluate the spatial resolution of the Pan-sharpened image.

Algorithm 3.1 The proposed Pan-sharpening algorithm

Input: HR PAN and LR MS image (Assume the size of the HR PAN image is four times larger than the LR MS image.)
Output: HR MS image

1. Take the real sketch graph to the original HR PAN image.
2. Downsample the real sketch graph and original HR PAN image, respectively. (The size of the downsampled sketch graph and the HR PAN image is one half of its original). According to the downsampled sketch graph and the downsampled HR PAN image, the regional map is obtained by the designed template.
3. Regional division. Interpolate the LR MS (IMS) image by the nearest interpolation method (the same size with the downsampled HR PAN image). Divide the IMS image into structure, texture and the smooth regions.
4. Learning interpolation. For each band of LR MS image, relearn and readjust the pixels in the structure regions by the structure learning interpolation method, the pixels in the texture regions by the texture learning interpolation method, and the pixels in the smooth regions by the average weighted interpolation method.
5. Interpolation the image obtained from step 4 by the nearest interpolation method, a new IMS image is obtained (the same size with the original HR PAN image). According to the real sketch graph and the real HR PAN image, repeat the learning interpolation process for the new IMS image to get the final Pan-sharpened image.

The method used to evaluate the spectral information of the Pan-sharpened results compares the degraded version of the Pan-sharpened results with the original LR MS image. In addition, the spatial metrics are extracted by using the Pan-sharpened and the original HR PAN images.

A. Selection of Threshold T (Divide the Nonstructure Regions Into Smooth and Texture Regions)

Three groups of experiments are done for the threshold selection. If the variance value for a region is less than threshold T, this region is considered as the smooth region, and the weight is set as $\vec{\alpha} = [0.25, 0.25, 0.25, 0.25]$ directly. In order to determine the threshold value, the HR PAN image and the Pan-sharpened images are filtered using a Laplacian filter, respectively. In addition, the correlation coefficients are computed between each filtered band of the Pan-sharpened image and the filtered HR PAN image. Through the filtering process, the detail information can be presented better in the filtered image. The larger the threshold value, the more blurred the Pan-sharpened images, and the average CC becomes less. Fig. 9(a)–(c) shows the CC statistic graph for the three groups of experiments. The abscissa is the variance value, and the ordinate is the correlation coefficients values. Moreover, Fig. 9(d)–(e) show the variance statistic graph. The abscissa represents the variance value, and the ordinate represents the pixel numbers. As shown

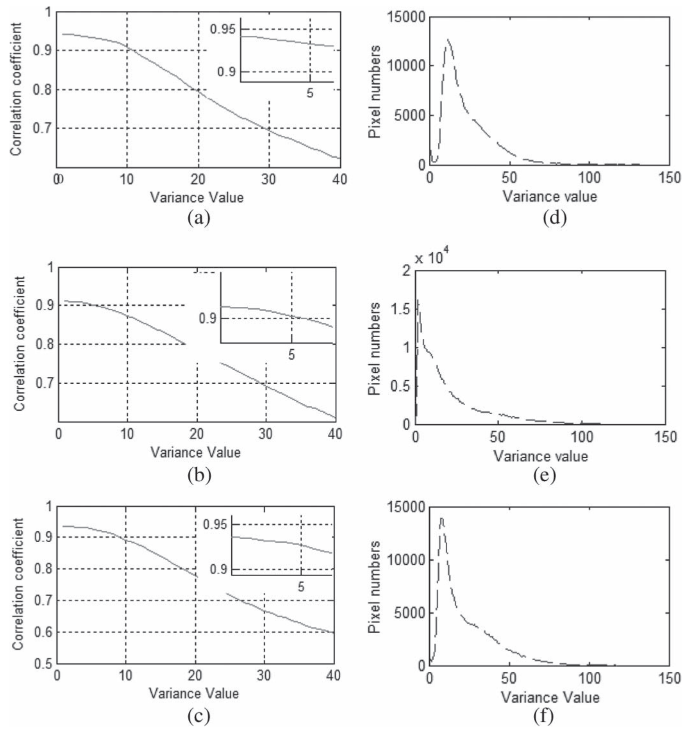

Fig. 9. Statistic map for the three group experiments. (a) CC statistic graph for the first group images. (b) CC statistic graph for the second group images. (c) CC statistic graph for the third group images. (d) Variance statistic map for the first group images. (e) Variance statistic map for the second group images. (f) Variance statistic map for the third group images.

in Fig. 9(d)–(e), most pixels have less variance values. Hence, a larger threshold value can reduce the computation complexity effectively. However, in Fig. 9(a)–(c), the spatial resolution of the Pan-sharpened image decreases with an increased threshold value. When the threshold value is equal to 5, all the CC values in the test images are larger than 0.9. In order to maintain a better spatial resolution, the threshold value is selected as 5 in this paper.

B. Comparative Experiments

To show the effect of the proposed Pan-sharpening algorithm, several different algorithms are compared with the proposed algorithm in their spectral and spatial quality, such as Traditional HIS [4], Adaptive IHS [8], PCA, Sparse FI [16], generalized Laplacian pyramids (GLPs) [36], Wavelet-based Pan-sharpening algorithm [10], UNB-PanSharp [37], and GS-based algorithm [7]. The IHS method is widely used because of its simple computation. In Figs. 10–13, the IHS method can improve the spatial resolution effectively; however, the spectral information is seriously distorted. Particularly in Fig. 11, this problem is even more serious. Similar to IHS method, this problem also appears in the PCA method. Hence, some modification algorithms have been proposed to enhance the spectral information, such as Adaptive IHS. The adaptive IHS method is proposed by Rahmani [8], and from Figs. 10(b) and 12(b), Adaptive IHS produces an image whose spectral information is maintained better than the traditional IHS method, but it is still not ideal. Sparse FI method depends on the trained dictionary, and therefore the results are not stable. In Figs. 10(d)–13(d), the sparse FI method always obtains a better spectral information, however, in Fig. 10(d), the spatial resolution is poor. MRA-based Pan-sharpening algorithm, GLP and Wavelet, can maintain better spectral information in the Pan-sharpened image, particularly for the GLP algorithm, the spatial resolution is maintained as well. Figs. 10–13(g) show the Pan-sharpened image by the UNB-Pansharp algorithm. This algorithm is used in a “Fuze Go” software. UNB-Pansharp has an excellent effect in spatial resolution, however, presents serious loss in the test dates. Similar to the UNB-Pansharp algorithm, the GS-based algorithm is also used in satellite software, such as ENVI. The Pan-sharpened image by the GS algorithm is obtained by the ENVI software. The phenomenon for spectral distortion still exists in the Pan-sharpened image. From the visual aspect, the proposed algorithm has the best effect in balancing the spectral and spatial resolution. It maintains the details clearer than other methods do, and meanwhile, the color is better matched with the LR MS image.

Tables I–IV show the quality metrics of different Pan-Sharpening methods. In Table I, Sparse FI method has a better quality metrics in spectral information. This is because the dictionary is trained only in the HR PAN and downsampled HRPAN image, but the first test image has few line features, and therefore, the trained dictionary cannot represent the image well. Hence, the Pan-sharpened image by Sparse FI method has a poor spatial resolution. Compared with other methods, the proposed Pan-sharpening algorithm reaches the optimum in most values. In these quality metrics, HIS, AIHS, PCA, UNB-Sharpen, and GS algorithm always have higher values in sCC value than the Wavelet and GLP algorithm. However, they fail to get the values in ERGAS, CC, SAM, and SID. Wavelet and GLP algorithm always obtain better values in spectral

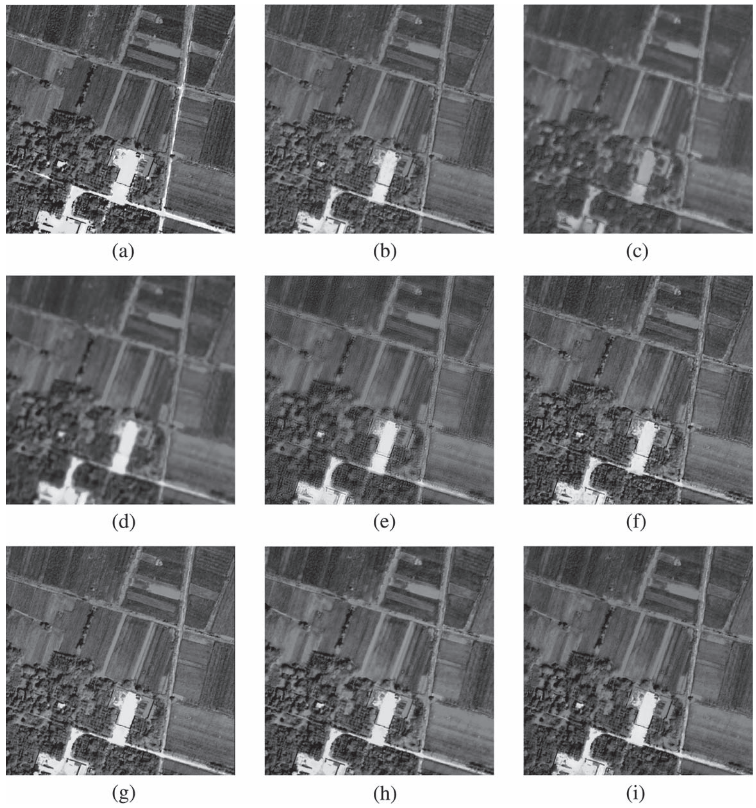

Fig. 10. Pan-sharpening results on dataset 1. (a) Traditional IHS. (b) Adaptive IHS. (c) PCA. (d) Sparse FI. (e) GLP. (f) Wavelet. (g) UNB-PanSharp. (h) GS. (i) Proposed.

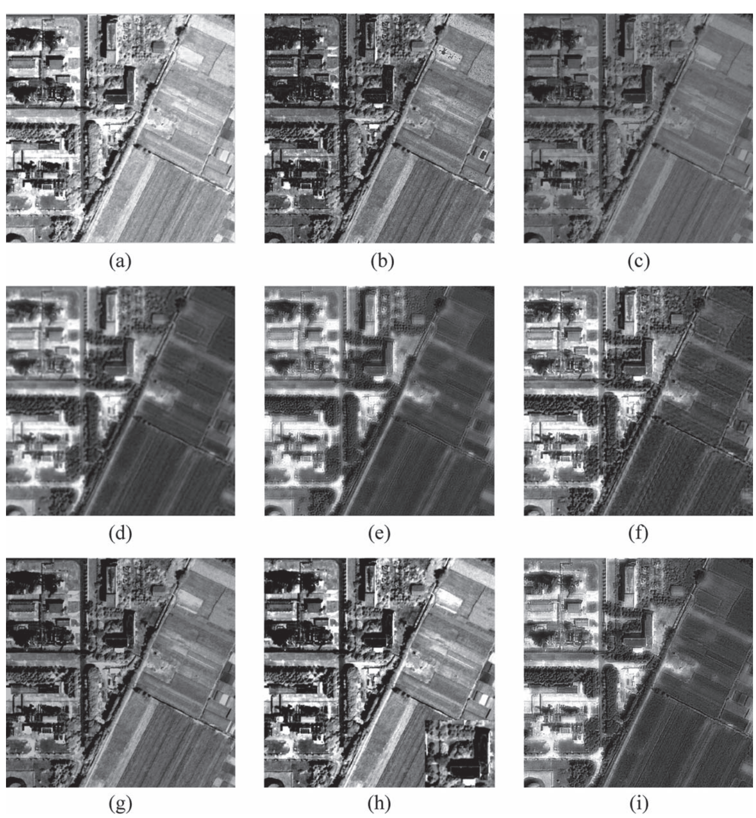

Fig. 11. Pan-sharpening results on dataset 2. (a) Traditional IHS. (b) Adaptive IHS. (c) PCA. (d) Sparse FI. (e) GLP. (f) Wavelet. (g) UNB-PanSharp. (h) GS. (i) Proposed.

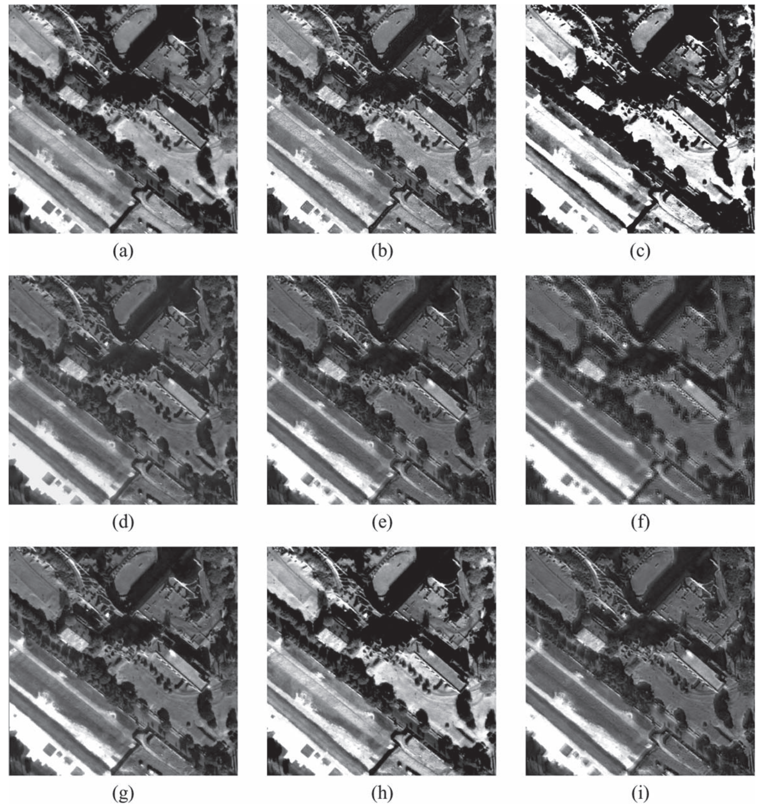

Fig. 12. Pan-sharpening results on dataset 3. (a) Traditional IHS. (b) Adaptive IHS. (c) PCA. (d) Sparse FI. (e) GLP. (f) Wavelet. (g) UNB-PanSharp. (h) GS. (i) proposed.

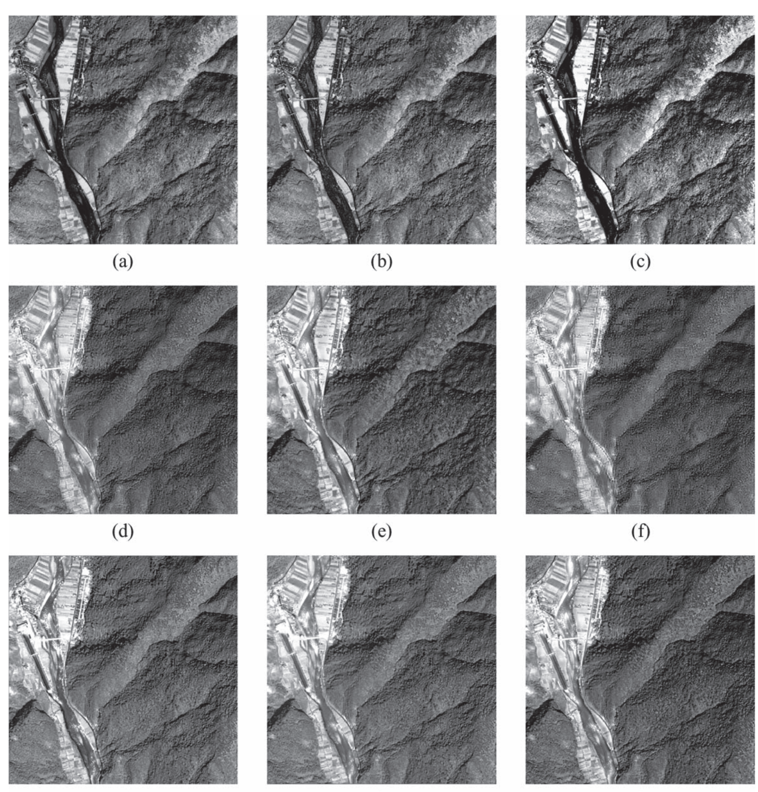

Fig. 13 Pan-sharpening results on dataset 4. (a) Traditional IHS. (b) Adaptive IHS. (c) PCA. (d) Sparse FI. (e) GLP. (f) Wavelet. (g) UNB-PanSharp. (h) GS. (i) Proposed.

TABLE I
QUALITY METRIC IN DATASET I

	ERGAS	CC	SAM	SID	PSNR	sCC
Best Values	0	1	0	0	$+\infty$	1
IHS	4.4593	0.8787	8.8617	0.2534	18.6738	0.8132
AIHS	3.8563	0.9159	2.0813	0.2837	21.9518	0.8877
PCA	7.2266	0.6073	21.8065	2.1444	15.5152	0.7613
Sparse FI	**2.3287**	0.9510	**1.6837**	0.0477	15.2684	0.2186
GLP	2.6871	0.9508	2.9998	0.0728	22.0517	0.9187
Wavelet	4.0556	0.8609	8.9972	0.5860	20.8035	0.8676
UNB-PanSharp	3.7594	0.8929	12.6883	0.2516	18.8695	0.9202
GS	3.8725	0.9024	11.3415	0.2056	20.3503	0.8131
Proposed	2.6173	**0.9514**	1.7228	**0.0425**	**23.9979**	**0.9251**

TABLE II
QUALITY METRIC IN DATASET II

	ERGAS	CC	SAM	SID	PSNR	sCC
Best Values	0	1	0	0	$+\infty$	1
IHS	5.2510	0.4430	7.3449	0.1840	9.1928	0.9217
AIHS	6.5428	0.3056	14.5449	0.1769	11.4376	0.9327
PCA	6.2581	0.3103	7.4447	0.2567	12.2954	0.9314
Sparse FI	2.3914	**0.9510**	3.8574	0.0418	21.1052	0.9361
GLP	2.5533	0.9479	3.8987	0.1919	22.4172	0.8249
Wavelet	2.5380	0.9224	3.7266	0.1249	20.1223	0.7242
UNB-PanSharp	7.2150	0.1758	15.6290	0.2039	10.4422	0.9328
GS	6.2373	0.3157	18.7107	0.2165	9.7761	**0.9415**
Proposed	**2.3571**	0.9422	**3.1774**	**0.0082**	**22.7498**	0.9353

TABLE III
QUALITY METRIC IN DATASET III

	ERGAS	CC	SAM	SID	PSNR	sCC
Best Values	0	1	0	0	$+\infty$	1
IHS	4.7097	0.7641	19.7087	0.4836	14.5437	0.9858
AIHS	4.6007	0.7671	12.6096	0.5797	14.3907	0.9878
PCA	7.1048	0.6381	40.6550	0.1666	9.7668	0.9862
Sparse FI	2.8285	0.9284	7.9172	0.3700	20.7410	0.9825
GLP	2.0851	0.9597	7.0922	0.2305	23.2611	0.9839
Wavelet	1.8227	0.9616	5.6624	0.2057	24.7426	0.9883
UNB-PanSharp	2.9271	0.9123	8.4291	0.2573	19.4102	0.9839
GS	4.7960	0.7769	24.2953	0.1317	13.4308	0.8890
Proposed	**2.0547**	**0.9638**	**4.2710**	**0.0960**	**23.6716**	**0.9952**

TABLE IV
QUALITY METRIC IN DATASET IV

	ERGAS	CC	SAM	SID	PSNR	sCC
Best Values	0	1	0	0	$+\infty$	1
IHS	5.5503	0.4364	10.0813	0.3384	12.8398	0.9936
AIHS	5.6546	0.4008	9.6739	0.3322	12.6237	0.9925
PCA	6.1342	0.4358	16.9040	0.2265	11.4973	0.9917
Sparse FI	2.9876	0.9034	5.6229	0.1965	18.1901	0.8720
GLP	2.7208	0.9139	4.9658	0.1779	19.0438	0.9904
Wavelet	2.3956	0.9083	5.4390	0.1842	18.1697	0.9922
UNB-PanSharp	3.0209	0.8297	8.3645	0.0658	16.5747	0.9932
GS	2.6036	0.8774	5.2805	0.0718	17.8756	0.9947
Proposed	**2.2322**	**0.9177**	**4.6021**	**0.0540**	**20.7629**	**0.9963**

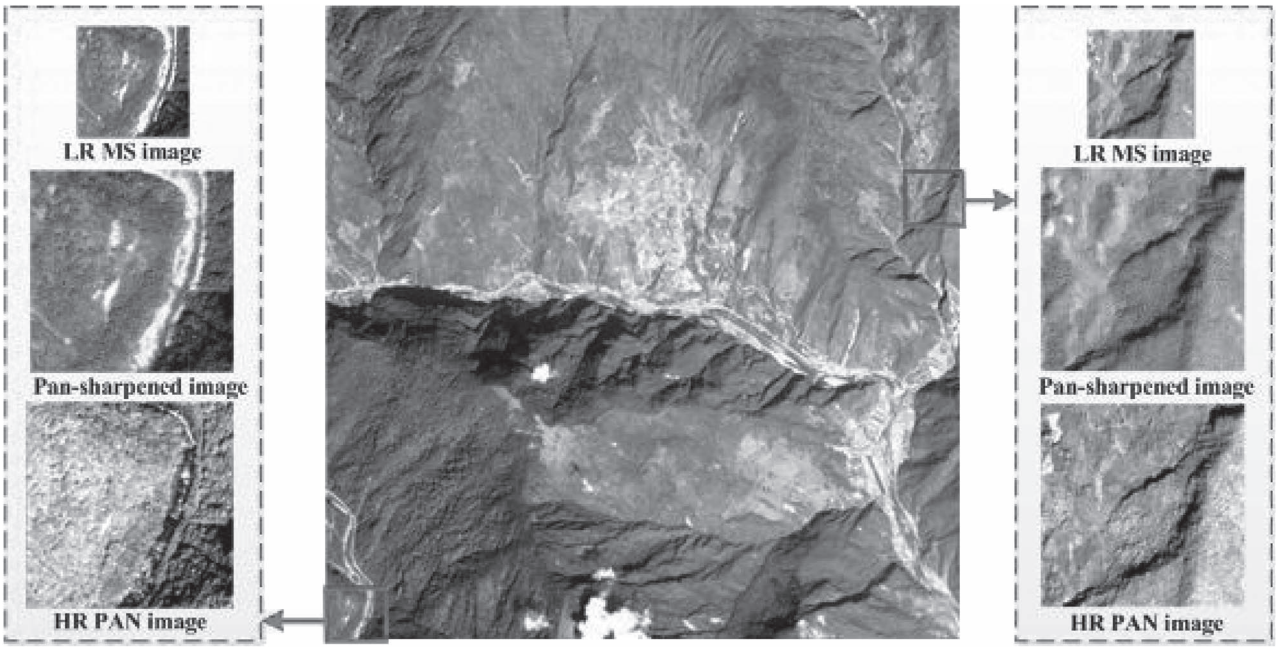

Fig. 14. Pan-sharpened IKONOS image by the proposed method.

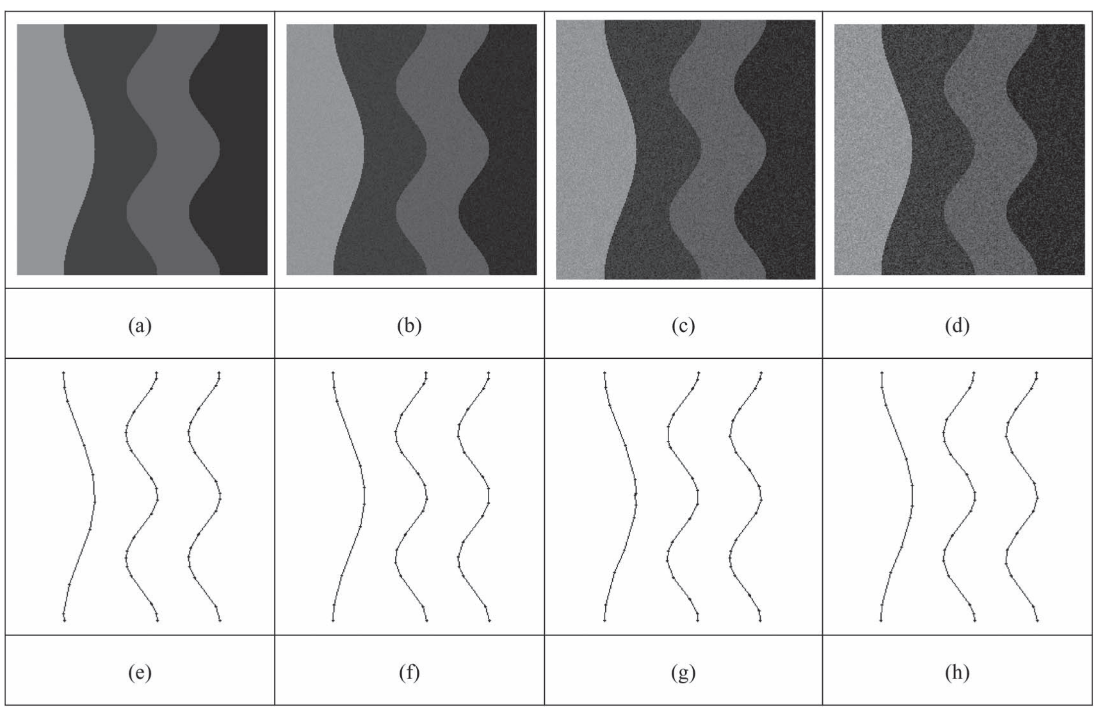

Fig. 15. Primal Sketch graph for synthetic image under different noisy conditions. (a) Original image with on noise. (b) Gauss noisy image with variance value as 5. (c) Gauss noisy image with variance value as 10. (d) Gauss noisy image with variance value as 15. (e) Primal Sketch obtained from the image (a). (f) Primal Sketch obtained from the image (b). (g) Primal Sketch obtained from the image (c). (h) Primal Sketch obtained from the image (d).

information. The proposed algorithm can get best values in most quality metrics. This can verify that the proposed learning interpolation algorithm for Pan-sharpening can achieve better results than other methods do.

To further verify improve the effectiveness of the proposed algorithm, the larger IKONOS LR MS and HR PAN images are shown in Fig. 14. The size of the LR MS image is 1000×1000, and the size of the HR PAN image is 4000×4000. The left and the right dashed box are the detail images for the red box parts. The whole Pan-sharpened image has better spectral information, and meanwhile, the spatial resolution is improved well.

C. Robustness for the Regional Map Under the Noisy Condition

The regional map is obtained according the Primal Sketch graph; hence, this experiment is to show the robustness for the

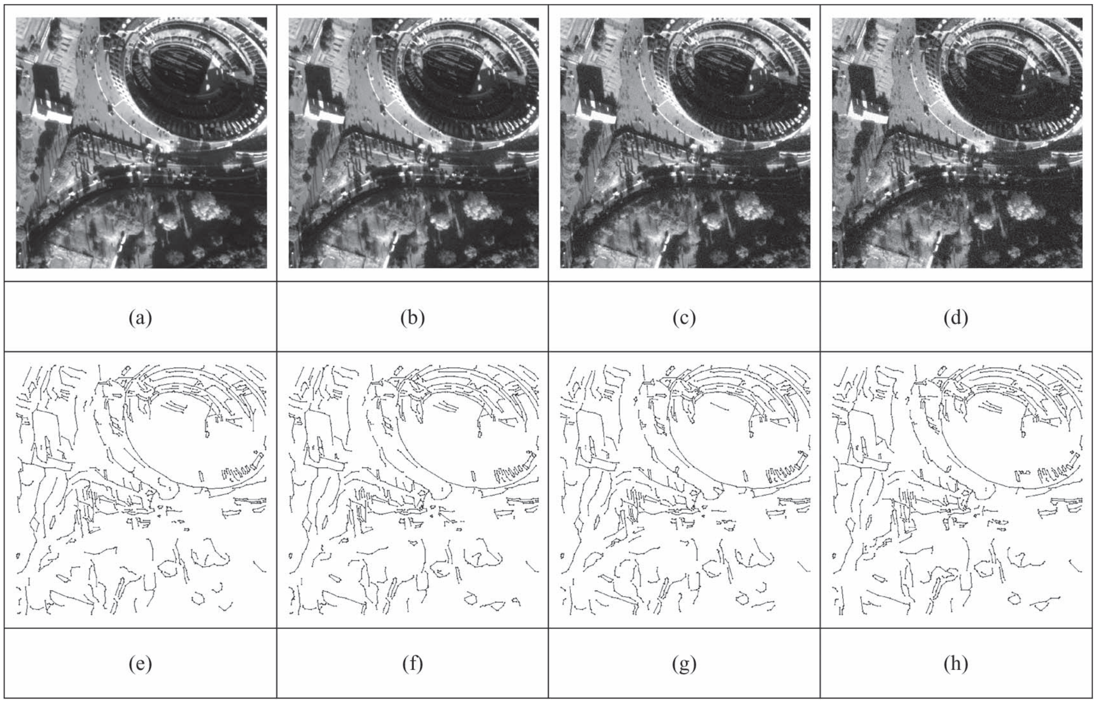

Fig. 16. Primal Sketch graph for HR PAN image under different noisy conditions. (a) Original image with no noise. (b) Gauss noisy image with variance value as 5. (c) Gauss noisy image with variance value as 10. (d) Gauss noisy image with variance value as 15. (e) Primal Sketch obtained from the image (a). (f) Primal Sketch obtained from the image (b). (g) Primal Sketch obtained from the image (c). (h) Primal Sketch obtained from the image (d).

Primal Sketch graph under the noisy condition. According to the steps for the Primal Sketch graph described in Section III, an analysis can be concluded that the initial sketch graph is similar to the canny edge detection algorithm, but not exactly the same. The filter used in the canny edge detection algorithm is only a subset of the primitives dictionary. As we all know, the canny edge detection algorithm has a better detection result when the noise in the image is additive noise. The filtering process is contained in the detection process to suppress the noise. In our paper, the Primal Sketch graph is obtained from the HR PAN image, under the most conditions, the noise is very moderate, and the noise is additive, hence the Primal Sketch graph is not affected when the noise is in the moderate levels.

Figs. 15 and 16 shows some experiments for verifying the correctness of the explanation. A synthetic image and a real HR PAN image are used as the test images. The noise added in the test image is Gauss noise with different variance values as 0, 5, 10, and 15. The noise in the HR PAN image is very moderate, and cannot be larger than 5 in variance value. From the results of the Primal Sketch graph, we can see that the Primal Sketch graph changes very little in different variance values. Particularly for the variance value that is less than 5, the Primal Sketch graphs are almost the same. Hence, in our proposed Pan-sharpening algorithm, the moderate noise cannot affect the accuracy of the regional division.

V. Concluding Remarks

The new algorithm of Pan-sharpening via learning interpolation is proposed in this paper. It is noted in this section that the HR PAN image is not injected into LR MS image to obtain the result. Combined with sketch information and regional maps, a fast-learning interpolation algorithm is designed to better keep spectral information. According to the gradient prior offered by an HR PAN image, the spatial resolution is effectively enhanced. It is proved by several groups of experiments that the proposed method can better balance the spectral information and spatial resolution. This is a new way for Pan-Sharpening the image, and it is very suitable for the images that have great differences in spectral information. The main disadvantage of the proposed Pan-sharpening algorithm consists of two parts: the imaging quality and the effectiveness of the noise. The proposed Pan-sharpening algorithm is based the spatial domain, and the computation for the adjustment parameter is dependent on the gradient of the HR PAN image. Hence, the imaging quality has some limitations to the proposed method. The imaging process is constrained in many ways, such as the atmospheric environment, or the imaging forming apparatus. Hence, before the Pan-sharpening process, some image preprocessing processes are necessary, such as image correction, image denoising, and image registration. When the image preprocessing is poor, or the preprocessing process is not ideal, the "spilling effect" in LR MS image, or the registration error may affect the Pan-sharpening results. Besides, the noise in the HR PAN image may affect the accuracy of the gradient calculation. When the noise is relatively small, this affect is not obvious, such as the test images in this paper. Moreover, the Primal Sketch graph and regional map are also not effect by the small noise. Better Pan-sharpening results can be obtained in our experimental results. However, when the noise is relatively large, some artifacts may appear in the

Pan-sharpened image. Hence, the proposed Pan-sharpening algorithm is suitable for the images with small noise. If the images have obvious noise, a denoising process is necessary before the Pan-sharpening process.

REFERENCES

[1] Z. Wang, D. Ziou, C. Armenakis, D. Li, and Q. Li, "Comparative analysis of image fusion methods," *IEEE Trans. Geosci. Remote Sens.*, vol. 43, no. 6, pp.1391–1402, Jun. 2005.

[2] P. Chavez, S. C. Sides, and J. A. Anderson, "Comparison of three different methods to merge multiresolution and multispectral data: Landsat TM and SPOT panchromatic," *Photogramm. Eng. Remote Sens.*, vol. 57, no. 3, pp. 311–316, Mar. 1991.

[3] M. Chikr El-Mezouar, N. Taleb, K. Kpalma, and J. Ronsin, "An HIS-based fusion for color distortion reduction and vegetation enhancement in IKONOS imagery," *IEEE Trans. Geosci. Remote Sens.*, vol. 49, no. 5, pp. 1590–1602, May 2011.

[4] Y. Zhang and G. Hong, "An HIS and wavelet integrated approach to improve pan-sharpening visual quality of natural colour IKONOS and QuickBird images," *Inf. Fusion*, vol. 6, no. 3, pp. 225–234, Sep. 2005.

[5] T. M. Tu, S. C. Su, H. C. Shyu, P. S. Huang, "A new look at HIS like image fusion methods," *Inf. Fusion*, vol. 2, no. 3, pp. 177–186, Sep. 2001.

[6] H. R. Shahdoosti and H. Ghassemian "Spatial PCA as a new method for image fusion," *Proc. 16th CSI AISP*, May 2012, pp. 090–094.

[7] C. A. Laben and B. V. Brower, Processing for enhancing the spatial resolution of multispectral imagery using pan-sharprning, U.S. Patent 6011875 A, Jan. 4 2000.

[8] S. Rahmani, M. Strait, D. Merkurjev, M. Moeller, and T. Wittman, "An adaptive HIS pan-sharpening method," *IEEE Geosci. Remote Sens. Lett.*, vol. 7, no. 4, pp. 746–750, Oct. 2010.

[9] C. Ballester, V. Caselles, L. Igual, J. Verdera, and B. Rouge, "A variational model for P+XS image fusion," *Int. J. Comput. Vis.*, vol. 69, no. 1, pp. 43–58, Aug. 2006.

[10] X. Otazu and M. Gonzalez-Ausicana, "Introduction of sensor spectral reponse into image fusion methods: Application to wavelet-based methods," *IEEE Trans. Geosci. Remote Sens.*, vol. 43, no. 10, pp. 2376–2385, Oct. 2005.

[11] A. Garzeli, F. Nencini, L. Alparone, and S. Baronti, "Multiresolution fusion of multispectral and panchromatic images through the curvelet transform," *Proc. IEEE IGARSS*, Jul. 2005, vol. 4, pp. 2838–2841.

[12] X. Qu, J. Yan, G. Xie, Z. Zhu, and B. Chen, "A novel image fusion algorithm based on bandelet transform" *Chin. Opt. Lett.*, vol. 5, no. 10, pp. 569–572, Oct. 2007.

[13] S. Y. Yang, M. Wang, L. C. Jiao, R Wu, and Z Wang, "Image fusion based on a new contourlet packet." *Inf. Fusion*, vol. 11, no. 2, pp. 78–84, Apr. 2010.

[14] V. P. Shah, N. H. Younan, and R. L. King, "An efficient pan-sharpening method via a combined adaptive PCA approach and contourlets," *IEEE Trans. Geosci. Remote Sens.*, vol. 46, no. 5, pp. 1323–1335, May 2008.

[15] S. Li and B. Yang, "A new pan-sharpening method using a compressed sensing technique," *IEEE Trans. Geosci. Remote Sens.*, vol. 49, no. 2, pp. 738–746, Feb. 2011.

[16] X. X. Zhu and R. Bamler, "A sparse image fusion algorithm with application to pan-sharpening," *IEEE Trans. Geosci. Remote Sens.*, vol. 51, no. 5, pp. 2827–2836, May 2013.

[17] T. Blu, P. Thevenaz, and M. Unser, "Linear interpolation revitalized," *IEEE Trans. Image Process.*, vol. 1, no. 3, pp. 710–719, May 2004.

[18] H. Hou and H. Andrews, "Cubic splines for image interpolation and digital filtering," *IEEE Trans. Acoust., Speech Signal Process.*, vol. 26, no. 2, pp. 508–517, Dec. 1978.

[19] T. M. Lehmann, C. Gonner, and K. Spitzer, "Addendum: B-spline interpolation in medical image processing," *IEEE Trans. Med. Imag.*, vol. 20, no. 7, pp. 660–665, Jul. 2001.

[20] L. Zhang and X. Wu, "An edge-guided image interpolation algorithm via directional filtering and data fusion," *IEEE Trans. Image Process.*, vol. 15, no. 8, pp. 2226–2238, Aug. 2006.

[21] K. Jensen and D. Anastassiou, "Subpixel edge localization and the interpolation of still images," *IEEE Trans. Image Process.*, vol. 4, no. 3, pp. 285–295, Mar. 1995.

[22] D. Zhou, X. Shen, and W. Dong, "Image zooming using directional cubic convolution interpolation," *IET Image Process.*, vol. 6, no. 6, pp. 627–634, Aug. 2012.

[23] A. Giachetti and N. Asuni, "Real time artifact-free image upscaling," *IEEE Trans. Image Process.*, vol. 20, no. 10, pp. 2760–2768, Oct. 2011.

[24] X. Li and M. T. Orchard, "New edge-directed interpolation," *IEEE Trans. Image Process.*, vol. 10, no. 10, pp. 1521–1527, Oct. 2001.

[25] D. Marr, *Vision*, New York, NY, USA: Freeman, 1982.

[26] S. C. Zhu, C. E. Guo, Y. Wang, and W. Xu, "What are textons?" *Int. J. Comput. Vis.*, vol. 62, no. 1, pp. 121–143, Apr./May 2005.

[27] W. Hu, H. Gong, S. C. Zhu, and Y. Wang, "An integrated background model for video surveillance based on Primal Sketch and 3D scene geometry," *Proc. IEEE Conf. Comput. Vis. Pattern Recognit.*, Jun. 2008. pp. 1–8.

[28] A. Buades, B. Coll, and J. M. Morel, "A non-local algorithm for image denoising," *Proc. IEEE Comput. Soc. Conf. Comput. Vis. Pattern Recognit.*, Jun. 2005,vol. 2, pp. 60–65.

[29] A. Buades, B. Coll, and J. M. Morel, "On image denoising methods," Tech. Note, CMLA, Cachan, France, 2004.

[30] Y. L. Liu, J. Wang, X. Chen, G. Yanwen, and Q. Peng, "A robust and fast non-local means algorithm for image denoising," *J. Comput. Sci. Technol.*, vol. 23, no. 2, pp. 270–279, Mar. 2008.

[31] X. Zhang, X. Feng, and W. Wang, "Two-direction non-local model for image denoising," *IEEE Trans. Image Process.*, vol. 22, no. 1, pp. 408–412, Jan. 2013.

[32] C. H. Lin, P. H. Tsai, K. H. Lai, and J. Y. Chen, "Cloud removal from multitemporal satellite images using information cloning," *IEEE Trans. Geosci. Remote Sens.* , vol. 51, no. 1, pp. 232–241, Jan. 2013.

[33] T. Ranchin and L. Wald, "Fusion of high spatial and spectral resolution images: The ARSIS concept and its implementation," *Photogramm. Eng. Remote Sens.*, vol. 66, no. 1, pp. 49–61, 2000.

[34] S. Chen, H. Su, R. Zhang, "The tradeoff analysis for remote sensing imagefusion using expanded spectral angle mapper," *Sensors*, vol. 8, no. 1, pp. 520–528, Sep. 2005.

[35] J. Saeedi and K. Faez, "A new pan-sharpening method using multiobjective partical swarm optimization and the shiftable contourlet transform," *ISPRS J. Photogramm. Remote Sens.*. vol. 66, no. 3, pp. 365–381, May 2011.

[36] B. Aiazzi, L. Alparone, F. Argenti, and S. Baronti "Wavelet and pyramid techniques for multisensor data fusion: A performance comparison varying with scale ratios," *Remote Sens. Int. Soc. Opt. Photon.*, vol. 3871, pp. 251–262, 1999.

[37] Zhang, Yun, and R. K. Mishra. "From UNB PanSharp to Fuze Go-the success behind the pan-sharpening algorithm," *Int. J. Image Data Fusion*. vol. 3, no. 1, pp. 39–53, 2014.

Cheng Shi received the bachelor's degree from the Xi'an University of Architecture and Technology, Xi'an, China. She is currently working toward the Ph.D. degree in computer application technology at Xidian University, Xi'an.

Her main research interests include multiscale geometric analysis, image processing, and information fusion.

Fang Liu (M'07–SM'07) received the B.S. degree in computer science and technology from Xi'an Jiaotong University, Xi'an, China, in 1984 and the M.S. degree in computer science and technology from Xidian University, Xi'an, in 1995.

She is currently a Professor with the School of Computer Science, Xidian University. She is the author or coauthor of five books and more than 80 papers in journals and conferences. Her research interests include signal and image processing, synthetic aperture radar image processing, multiscale geometry analysis, learning theory and algorithms, optimization problems, and data mining.

Lingling Li received the B.S. degree from the School of Electronic Engineering, Xidian University, Xi'an, China, where she is currently working toward the Ph.D. degree in the School of Electronic Engineering, Xidian University.

Her current research interests include community detection in networks and multiobjective optimization.

Licheng Jiao (SM'89) received the B.S. degree from Shanghai Jiaotong University, Shanghai, China, in 1982, and the M.S. and Ph.D. degrees from Xi'an Jiaotong University, Xi'an, China, in 1984 and 1990, respectively.

He is currently a Distinguished Professor with the School of Electronic Engineering, Xidian University, Xi'an. He has led approximately 40 important scientific research projects and has published more than ten monographs and 100 papers in international journals and conferences. He is the author of three books: *Theory of Neural Network Systems* (Xidian University Press, 1990), *Theory and Application on Nonlinear Transformation Functions* (Xidian University Press, 1992), and *Applications and Implementations of Neural Networks* (Xidian University Press, 1996). He is the author or coauthor of more than 150 scientific papers. His research interests include signal and image processing, natural computation, and intelligent information processing.

Prof. Jiao is a member of the IEEE Xi'an Section Executive Committee and the Chairman of the Awards and Recognition Committee and an executive committee member of the Chinese Association of Artificial Intelligence.

Yiping Duan received the B.S. degree from the School of Computer, Henan Normal University, Henan, China. She is currently working toward the Ph.D. degree in the School of Computer, Xidian University, Xi'an, China.

Her current research interests include semantic mining, machine learning, and synthetic aperture radar image processing.

Shuang Wang (M'07) was born in Shannxi, China, in 1978. She received the B.S., M.S., and Ph.D. degrees from Xidian University, Xi'an, China, in 2000, 2003, and 2007, respectively, all in circuits and systems.

She is currently a Professor with the Key Laboratory of Intelligent Perception and Image Understanding of the Ministry of Education of China, Xidian University. Her main research interests are image processing, machine learning, synthetic aperture radar (SAR), polarimetric SAR image processing, etc.